CHAPTER 9: LASER SYSTEMS

TRIVENI RAO
Brookhaven National Laboratory
Upton, NY 11973
THOMAS TSANG
Brookhaven National Laboratory
Upton, NY 11973

Keywords
Diode Pumped Solid State Laser, Ti:Sapphire Laser, Fiber Laser, Mode-Locking, Phase Locking, RF-Laser Synchronization, Laser Shaping, Temporal Shaping, Spatial Shaping

Abstract
The laser system for the photoinjector is selected based on the cathode material and the electron beam parameters required for the application and hence can vary widely. This chapter is aimed not at describing one system in detail, but to give an overview of the options available. We encourage the readers to seek additional in-depth material by reviewing the references provided in this chapter. Since in majority of the systems, the general architecture typically is of Master Oscillator Power Amplifier (MOPA) configuration, we provide an overview of each of its components and their different operating modes. We then describe two most commonly used diode-pumped-solid-state (DPSS) laser systems: Nd: Vanadate and Ti: sapphire, as examples of the MOPA. Since the fiber lasers are gaining popularity, especially for high average current applications, their capabilities are also described. Irrespective of the exact configuration, all these photoinjector lasers have to meet a set of general conditions such as delivering the properly shaped beam at the correct time and energy with tight tolerance. We address this by discussing different beam shaping techniques, beam transport, synchronization and diagnostics.

9.1 INTRODUCTION

In previous chapters, we showed that the quantum efficiency (QE) and the photon energy required to overcome the work function for different cathode materials vary significantly.
Table 9.1 lists the photocathode materials used in various operating photoinjectors, the photon energy of the laser used, and the laser energy required to release a 1 nC charge.

Cathode Material	QE/Photon Energy	Laser Energy for 1 nC
Copper	1.4×10^{-4}/4.96 eV [9.1]	35.4 μJ
Magnesium	5×10^{-4}/4.66 eV [9.2]	9.2 μJ
Lead	2.7×10^{-3}/5.8 eV [9.3]	2.2 μJ
Cs_2Te	0.092/4.66 eV [9.4]	51 nJ
K_2CsSb	0.1/2.33 eV [9.5]	23.3 nJ
GaAs:Cs, non-polarized	0.1/2.33 eV [9.6]	23.3 nJ
GaAs:Cs, polarized	0.01/1.47 eV [9.6]	147 nJ

Table 9.1. Photocathode materials used in existing photoinjectors, their respective QE, and the laser energy required to release 1 nC from the cathode.

In this section, we highlight the architecture of the laser system capable of delivering the required specifications to the cathode at the appropriate wavelength. In order to assure a stable electron beam operation with the highest energy and minimum emittance, most RF injectors require that the repetition rate of the laser be phase-locked, either to the fundamental RF frequency of the injector that ranges from tens of megahertz to a few gigahertz or to a harmonic/sub-harmonic frequency of the injector. Furthermore, the laser may also need to run in the macro/micropulse mode, depending on the application.

In order to reduce the emittance growth related to RF fields, the pulse duration of the laser is typically a few degrees of the RF cycle. To reduce the energy fluctuation and maintain the longitudinal emittance of the electron beam the timing jitter should be of less than one degree of the RF cycle. The shortest pulse duration that the injector can accommodate is determined by the space charge limit imposed by the peak current and the transit time of the electron bunch in the cathode material. For a metal cathode with the electron velocity of ~3 500 m s^{-1} and absorption length of ~1 nm, the transit time is ~285 fs. Hence, laser beams with a shorter pulse duration would not produce correspondingly shorter electron bunches. Furthermore, a nanocoulomb bunch charge with such a short pulse duration corresponds to a peak current of 3 500 A, which is well above the space charge limited regime, even in the presence of 100 MV m^{-1} gradient field.

In a RF gun, the transverse spatial size of the electron beam is optimized to minimize the emittance growth due to RF and space charge effects. The space charge effects are proportional to the charge density, favoring a larger electron beam diameter for a given charge. However, the RF effects dictate that the radius of the electron beam should be well within the region wherein the accelerating field is normal to the cathode. In typical RF injectors, the electron beam's size, and hence the spatial laser beam size, are adjusted to < 1% of the RF wavelength in order to minimize the growth of transverse emittance; the laser pointing stability is usually kept within a few percent of this spot size.

Numerous simulations [9.7], [9.8] indicate that the emittance of the electron beam from the injector can be minimized by shaping the electron beam, and hence the laser beam, both transversely and longitudinally. Once again, the electron beam and the RF parameters dictate its exact dimensions.

9.2 LASER ARCHITECTURE

In general, the parameters of the laser systems driving the photoinjectors, such as the gain medium, energy, peak power, average power, repetition rate and pulse structure, are determined by the cathode and the electron beam characteristics for the intended application which can cover a wide range. The exact configuration of the laser system is application specific. In this section, we address only the general architecture and different options that are available. We evaluate their advantages and disadvantages. Only pulsed lasers are discussed since they are more relevant to the photoinjectors. We note that the laser field is evolving rapidly, making technical details obsolete rather quickly. Hence, different laser media are discussed only in terms of their fundamental properties that are relevant to the photoinjectors.

Before choosing a suitable laser system, the following characteristics must be specified based on the electron parameters and the cathode of choice: Laser wavelength, repetition rate, polarization, transverse- and longitudinal beam profile, pulse energy, pulse duration, pulse structure, pulse stability, pointing stability, timing accuracy and tolerance to the presence of pre/post pulse.

In most cases, the typical architecture is in the form of Maser Oscillator Power Amplifier (MOPA) arrangement. The weak light pulse generated from a laser master oscillator is increased in the subsequent amplifiers. The gain media in the master oscillator and the amplifier determine the laser wavelength and the

shortest possible pulse duration. The upper state's lifetime and energy storable in this gain media, along with the damage threshold of the optics, dictate the maximum extractable energy and power from the system. Typically the master oscillator can meet most of the requirements of the photoinjector other than the pulse energy and the average power. Power amplifiers are used to increase the pulse energy and the average power without compromising overall performance. Additional optical elements are usually inserted in the system to tailor the light pulses for other needs, such as improvement of the signal-to-noise ratio, scribing micro/macropulse structure, and transforming the transverse- and longitudinal-beam profile.

9.2.1 Master Oscillator

The basic components of a laser oscillator are the gain medium, a pump source that excites the gain medium to the upper state of the lasing levels and a pair of high reflectivity mirrors on either side of the gain medium to form the laser cavity. Passage of the optical beam at the lasing wavelength through the gain medium increases its photon density, but is counteracted by the internal losses in the cavity, such as the scattering in the mirrors and absorption in the gain medium. The system oscillates when the gain in the cavity equals the total losses. The transverse parameters of the laser output are determined by the resonator geometry comprising of the mirrors, their placement and the overlap of the pump profile with the transverse electromagnetic fields supported by the laser resonating cavity. The cavity can be made to oscillate in a diffraction-limited single transverse mode, such as TEM_{00} (Gaussian spatial distribution), by carefully choosing the geometry of the resonator and the pump beam. For a non-diffraction limited beam, the beam's quality factor M^2 (defines as θ/θ_G where θ and θ_G are, respectively, the far-field divergence angles of the non-diffraction limited beam and the Gaussian beam) quantifies the deviation from a true Gaussian beam. The spectral distribution of the gain medium and the resonator define the spectrum of the laser output.

The temporal characteristics of the laser beam are dictated by the temporal behavior of the gain $g(t)$ and loss $\alpha(t)$ of the system; in steady-state, they are equal. However, by modulating $g(t)$ and $\alpha(t)$ a stable pulsed operation can be maintained. The gain can be adjusted by modulating the pump power. Some examples are flash lamp pumping and discharge pumping of the lasers, current modulation in a semiconductor laser [9.9]–[9.11], and synchronous pumping in a dye laser [9.12], [9.13]. Examples of the loss modulation include Q-switching, cavity dumping, and active or passive mode-locking. We discuss the general principles of Q-switching and mode-locking in the sub-section below. Current modulation that is specific to semiconductor lasers is described in Chapter 8. We will omit the discussion on older technologies of the synchronous pumping of dye laser and discharge pumping of excimer lasers, since they are not widely used in photoinjector applications. In most applications, flash lamp pumping was replaced by diode pumping, and hence, it will not be discussed either.

9.2.1.1 Q-Switching

The onset of laser oscillation occurs when the gain in the system equals the loss. Considering a laser cavity with a shutter, when the shutter is closed, the loss in the system is large and the Q of the cavity, *i.e.*, the ratio of the energy stored in the cavity to the energy loss per cycle, is small. When the gain medium is pumped to reach population inversion, the stored energy and the gain in the medium reach a high value without the onset of laser oscillation. If the shutter is quickly opened, the Q of the cavity suddenly switches to a high value so that the gain in the cavity far exceeds the loss and the stored energy can be released in an extremely short time. The time for which the energy can be stored in the gain medium is on the order of the upper state lifetime of the lasing levels. The pulse duration of the laser output is of the order of a few round-trip times of the laser cavity. Since this process involves fast switching of the Q of the cavity from low to high value, it is known as Q-switching [9.14]. Q-switching can be accomplished using acoustic-optic and electro-optic

crystals [9.15]–[9.18] and saturable absorbers [9.14], [9.19]–[9.22] covering MHz to a few Hertz repetition rate.

When a laser is pumped continuously with repetitive Q-switching, many of the laser characteristics such as the peak and average power, pulse duration (longer at higher repetition rates) and the spatial beam quality are strongly influenced by the integrity of this repetitive switching. The pumping can be in the pulsed mode arriving shortly before the opening of the Q-switch, but strong enough to saturate the population inversion. Some drawbacks of this Q-switch technique are pre- and post-lasing due to the finite Q value, double-pulsing due to excessively high gain, and fast modulation of the Q-switched envelope due to multiple resonator modes supported in the cavity. However, employing the technique of injection seeding has resolved many of these issues, as detailed in [9.14]. The duration of the laser pulse is about a few round-trip times of the cavity typically in nanoseconds: the energy per pulse can be in the range of a few millijoules, making it an attractive, lower cost option. Shorter pulse durations can be obtained by Q-switching in pulse-transmission mode. In this scheme, the circulating power is allowed to build up in the cavity made up of 100% reflecting mirrors. At its peak, the reflectivity of one mirror is switched from 100% to 0% (transmission from 0% to 100%), thereby emitting the entire cavity's optical power. Depending on the length of the cavity, pulse durations ranging from 1-5 ns are feasible with such devices. Q-switched lasers delivering > 2 J of energy in a few nanoseconds duration with average powers of tens of watts are commercially available [9.23].

Cavity dumping, a mechanism similar to Q-switching, can be employed for obtaining shorter pulses at higher repetition rates. While in Q-switching, energy storage is primarily achieved *via* atomic population inversion; in cavity dumping, it is *via* the cavity's optical field. In this scheme, the intra-cavity power is built to a high value in a high Q cavity. A modulator inserted at the focus of the beam extracts the beam from the cavity by modulating the direction of its diffracted beam. Cavity-dumped Nd:YAG laser with repetition rates from 125 kHz to several megahertz and pulse duration to 25 ns have been built [9.24], [9.25].

9.2.1.2 Mode-Locking

The shortest pulse obtainable from a laser cavity is the transform limit of the broadest bandwidth that the cavity can support. If we assume that all other optical elements in the cavity are broadband, an assumption justified for lasers operating with transform-limited pulse durations > 1 ps, then the inherent limitation stems from the bandwidth of the gain medium (the Ti:sapphire laser, with a bandwidth broad enough to support femtosecond pulse duration, is an exception to this condition). Since the laser cavities are much longer than the optical wavelengths, a typical laser cavity can simultaneously support hundreds of axial modes. In the frequency domain, the output contains a large number of discrete spectral lines spaced by the inverse of the round-trip time t_R in the cavity. If the gain bandwidth of the cavity is $\Delta\nu_L$, the number of axial modes, N, within this bandwidth is $\Delta\nu_L * t_R$. These modes oscillate independently and their phases are distributed randomly. In a mode-locked laser, these modes are constrained to have fixed phase relationship to each other; hence, their amplitude in the frequency and time domains has a well defined distribution. This constraint is imposed by introducing a repetitive intra-cavity loss modulator with a period equal to an integral multiple of the cavity's round-trip time. The lasing then takes place around the minimum of the loss modulation and the duration of individual mode-locked pulses is $\sim(t_R * N^{-1})$ [9.26]. This mode-locking is accomplished, in general, either passively with saturable absorbers [9.27]–[9.29] or actively [9.30], [9.31] with an amplitude or phase modulator. Commercial, mode-locked, diode-pumped solid-state (DPSS) lasers are readily available with average power in excess of 50 W, pulse duration of ~15 ps and repetition rates in the range of 50-100 MHz [9.23].

In a passively mode-locked laser, the amplitude of the strongest pulse from the noise is selectively emphasized, while the background noise is not. Since the timing of this pulse in the noise floor is random, if uncorrected, the laser output has a large timing jitter. In a drive laser for the photoinjector, the arrival time of the electron bunch, and hence the repetition rate of the laser, must then be synchronized accurately to an external RF clock to minimize timing jitter between laser and electron pulses. When saturable absorber such as SESAM mirror is used as a passive mode-locker and the cavity length of the laser oscillator must be actively controlled for phase-locking the RF frequency or its harmonics to the laser repetition rate. More in-depth discussion on this phase-locking technique appears later. With an active mode-locking, the synchronization is assured by matching the frequency of the modulator directly to the frequency of RF clock or its harmonic.

9.2.2 Power Amplifier

The low single-pulse energy from the oscillator is amplified with a series of power amplifiers. The number of amplifiers depends on the seed energy, the total energy required, the gain per amplifier, the acceptable signal-to-noise ratio (S/N) and the damage threshold of the components, especially the gain medium. Typical bulk oscillators run at ~100 MHz repetition rate with energy per pulse in the tens of nanojoules regime. As established in earlier chapters, to deliver nanocoulomb charge, this energy has to be increased to the microjoules regime in the UV for a metal photocathode of 0.1% QE, or to tens of nanojoules at 530 nm for GaAs or multialkali photocathodes. The S/N of the laser is not a significant concern in low average current injectors using metal photocathodes since the beam loss is not a big issue and the nonlinear conversion from IR to UV wavelength increases S/N significantly. The damage threshold is not a vital issue for delivering nanocoulomb charge at low repetition rates. However, for high average current, high repetition rate injectors, a high S/N is a key consideration in the laser design. Since the current generated from the noise has multiple deleterious effects, this current dilutes the beam quality; its trajectory does not follow that of the main beam, leading to unplanned beam loss and associated radiation and vacuum problems. These injectors require a S/N exceeding 10^6 or better.

As in the oscillator, the amplifier's architecture also varies significantly from system to system. However, a few general considerations are valid for all of them. The primary interest in designing the amplifier is the gain and its efficiency in energy extraction. At low signal levels, the energy in the amplifier increases exponentially with the length of the gain medium. However, as the energy increases, its extraction affects the population in the upper laser level and eventually reaches a point where the driving signal depletes inversion density. At this saturation level, the gain is linear to the length of the gain medium. Operating the amplifier just above this saturation level minimizes the energy fluctuation. However, this could alter the spatial and temporal profile of the seed radiation. The design of the amplifier should take into account the distortions that can be introduced into the seed pulse during amplification. Some causes for spatial distortion are non-uniformity in pumping and the intrinsic and extrinsic anisotropy of the gain medium, gain saturation in the central part of the cylindrically shaped pump beam with exponential growth on the outer edge of the cylindrical region, diffraction due to the finite size of the gain medium, and lensing effects due to non-uniform temperature distribution of the gain medium. The temporal profile of the amplified pulse might deviate from the seed pulse due to time-dependent population inversion, finite bandwidth of the gain medium and nonlinear effects caused by the high intensity of the amplified beam. In the case of a chirped seed pulse, the frequency (time) dependent gain can also modulate the spectral distribution of the beam, thus its temporal distribution. Energy released outside the beam's spatial- and temporal-structure adds to the system's noise. Care should be taken to avoid feedbacks into the amplifiers to prevent damage, pre-lasing and spurious noise signals.

The amplifier system can be either a series of linear amplifiers, regenerative amplifiers, or a combination of both. In a regenerative amplifier, the seed-pulse is injected in a resonant cavity containing the excited gain medium. After several passes through the medium and the corresponding increase in energy, the pulse is ejected from the cavity typically by a Pockels cell [9.32]. The delay between the injection- and extraction-time determines the number of passes through the gain medium, as well as the highest repetition rate that the amplifier can support. Since the seed pulse is amplified by the gain medium several times, the overall gain is high. In this arrangement, the mode quality of the injected beam is matched to the cavity's mode; the transverse profile of the amplified beam is dictated by the regenerative amplifier which can be maintained at a high quality. However, parasitic lasing could lower the S/N and gain-narrowing could reduce the bandwidth of the amplified pulse, both effects must be addressed carefully. The pulse duration of the seed pulse must be considerably shorter than the cavity's round-trip time; accordingly, this scheme is more applicable to amplifying picosecond or shorter duration pulses, but not longer ones. The switching speed in the cavity and the Pockels cell limit the maximum repetition rate, typically to around 100 kHz. The resonant condition also limits the spot size to a single value, and its associated damage threshold dictates the maximum extractable energy. To mitigate damage in high peak power laser systems, the seed pulse is often stretched in time, amplified and then recompressed after extraction. Typically, the stretching process introduces up-chirp or down-chirp to the seed pulse, and hence, the technique is called chirped pulse amplification (CPA) [9.33]. Hundreds of kilohertz repetition rates [9.34] and Joules of energy [9.35] (although not necessarily simultaneously) are possible with CPA amplification. Ever higher repetition rate approaching MHz systems are recently introduced in the market. Pulse energies of millijoules in tens of kilohertz are available with moderately sized systems.

In a linear multi-pass amplifier, the seed beam passes through an excited gain medium one or more times, increasing energy at each pass. The stored energy in the medium, the layout of the optics and the damage threshold govern the number of passes. Since the gain medium is not a part of a resonant cavity, mode-matching is not essential and the amplified spatial mode is merely dictated by the seed pulse. However, good overlap with the pump beam is important for maximum efficiency and minimum ASE. The optics can be arranged such that the spot size of the seed radiation increases with the beam energy, minimizing saturation and damage problems. Also, with a higher seed pulse energy, a gain medium with larger aperture can be used. It is important that the profiles of the pump and the seed beams be properly matched to assure maximum energy extraction and minimum deviation of the amplified beam from the seed distribution. An average power of > 50 W was obtained at repetition rates up to 750 MHz [9.36] with a Nd:Vanadate slab as the gain medium in the amplifier. Although laser systems with peak powers of petawatts were built in several laboratories [9.37]–[9.39] and are commercially available as custom designs, their peak power is too high and repetition rates too low to be relevant for producing photoelectrons in conventional injectors.

We discuss part of the laser's architecture, specifically the pulse selection, timing synchronization, beam shaping, harmonic generation and beam transport in the subsequent sections.

9.3 BULK SOLID STATE LASER SYSTEMS: $\lambda > 1$ μm

One of the most common gain media used in the photoinjector applications is Nd based glass or crystal. Several vendors market DPSS Nd lasers that are in a mature developmental state. Some Yb based systems under development are expected to deliver > 100 W average power with pulse duration of ~10-50 ps and repetition rates ranging from a few hundred kilohertz to gigahertz. In the following sections, we describe their common features, capabilities and limitations.

Table **9.2** lists some of the bulk solid state (BSS) laser systems, their operating wavelengths, and pulse durations. The narrow gain bandwidth of the Nd in crystalline host materials limit the pulse duration to a few picoseconds. Shorter pulse duration, > 60 fs, is obtained with non-crystalline glass lasers.

Host	**Dopant**	**Wavelength [μm]**	**Band Width [nm]**	**Gain Cross Section [$\times 10^{-20}$ cm^2]**	**Upper State Lifetime [μs]**
YAG	Nd	1.064	0.6	33	230
YLF	Nd	1.047-1.0530	1.2	18	480
Vanadate	Nd		0.8	300	100
Phosphate Glass	Nd	1.0535-1.054	24.3	4.5	323
KGW	Yb	1.026	25	2.8	250
YAG	Yb	1.030	6.3	2.0	950
Phosphate Glass	Yb	1.06-1.12	62	0.049	1 300
Sapphire	Ti	0.790	230	41	3.2

Table 9.2. Selected list of BSS laser systems and their operating parameters [9.40].

Figure **9.1** is a schematic of the laser system commercially developed for driving the ERL photoinjector at BNL. Although this system's parameters are specific for this application, several features are common to all drive lasers; hence, we give a detailed description of this system here.

The ERL laser system is designed to deliver up to 5 W at 355 nm, with pulse duration of ~10 ps, repetition rate of 9.38 MHz, synchronized to an external 703.5 MHz master clock with a sub-picosecond timing jitter. A pulse selection system is incorporated to allow the ramp up from a single pulse to a series of micropulses in a macropulse with variable repetition rate (up to 10 kHz), and ultimately, to a quasi-continuous 10 MHz to facilitate the recovery of electron energy in the LINAC.

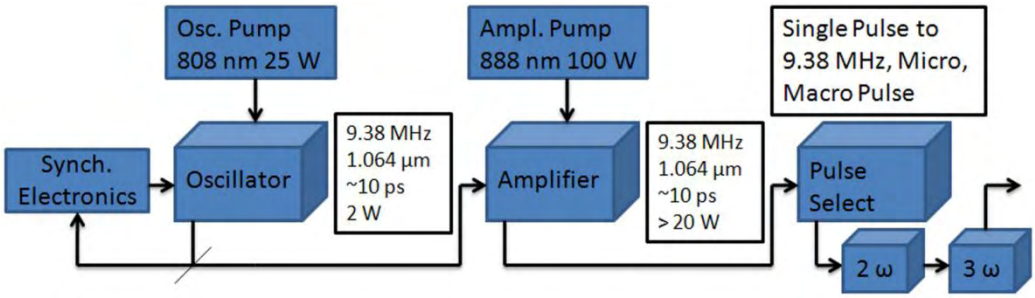

Figure 9.1. Schematic of commercial laser system developed for the ERL photoinjector at BNL. Note that some parameters are given; however, parameters are application specific.

9.3.1 Oscillator

The oscillator consists of a Nd:Vanadate crystal, a resonant cavity formed by a saturable absorber mirror (SAM) and an output coupler with 12% transmission. The 4×4×6 mm^3 laser crystal is end-pumped by 18 W fiber-coupled, diode laser, operating at 808 nm. The key feature of the oscillator is its repetition rate, too low for conventional CW mode-locking and too high for cavity dumping. To meet the challenge, a folded cavity with a resonator length of 16 m was custom-designed and built. Such a long cavity makes the laser very sensitive to misalignments compared to the conventional ~1 m long resonators. To isolate the oscillator

from mechanical- and thermal-instabilities, the oscillator is built on a monolithic metal-block and is sealed off from the rest of the system. The SAM is mounted on a stepper motor-driven translational-stage with 25 mm travel range to accommodate slow drifts in the cavity length and to coarse tune the repetition rate of the laser. A small mirror that is a part of the resonant cavity is mounted on a piezo-driven stage with 9 μm travel range to compensate for fast changes in the cavity length and to preserve synchronization. The output of the oscillator is extracted through an AR-coated window. A camera mounted behind one of the cavity mirrors continually monitors the beam's profile and position.

Figure **9.2** is a schematic for synchronizing the oscillator to the master clock. The photodiode signal from the laser and the signal from master clock, down-converted to 9.38 MHz, are fed into a phase detector. The output signal is further amplified and used to drive the stepper motor and the piezo stages in the oscillator.

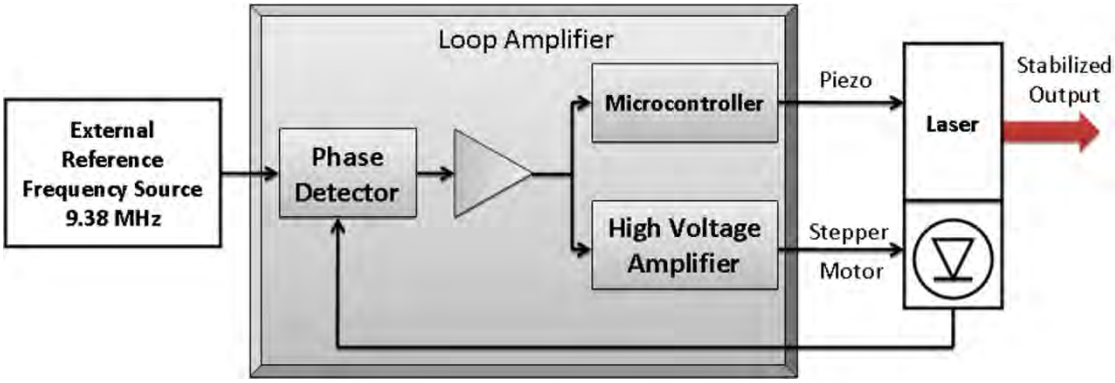

Figure 9.2. Schematic of the lock to clock system used in BNL's ERL laser.

9.3.2 Multipass Amplifier

The double-pass amplifier consists of a Vanadate crystal pumped by a 100 W diode laser operating at 888 nm. The weaker absorption at this wavelength reduces thermal problems, allowing a much higher pump power. The unabsorbed pump power in the first pass is reflected back into the crystal. A thin film polarizer that reflects vertical polarization and transmits horizontal polarization is inserted into the beam. A Faraday rotator changes the seed beam's polarization from vertical to horizontal after its second pass in the amplifier. The combination of thin film polarizer and the Faraday rotator allows the seed beam injection and amplified beam extraction out of the amplifier. The entire pulse train from the oscillator is amplified to eliminate the time-dependent changes in the thermal load induced by the seed- and amplified-pulses. The power and profiles of seed and amplified beams are monitored continually using the leakage signals at multiple locations. An optical isolator at the input end prevents feedback from the amplifier entering the oscillator. With 100 W pump power, > 20 W amplified power at 1.064 μm was delivered from the amplifier. Figure **9.3** Figure **9.4**, Figure **9.5** and Figure **9.6** display some performance characteristics of the amplified beam.

9.3.3 Pulse Selector

The pulse selector changes the repetition rate during the ramp-up process for the ERL and also alters its average current without changing the bunch charge. Since the S/N is an important consideration for the high current ERL, two significant changes were made to the conventional scheme: Since BBO can withstand a constant high voltage and can be oriented for the best contrast, it is used as the Pockels cell; and, the pulses are picked by the polarizing beam-splitter cube (PBS) when the voltage is applied to the Pockels cell, rather than when it is turned off. The high voltage is triggered externally to deliver pulses from single shot to a micro/macropulse configuration with variable number of micropulses within a macropulse and macropulse

repetition rate variable up to 10 kHz. However, the entire 9.38 MHz pulse train also can be delivered to the cathode. A few selected pulse configurations are illustrated in Figure **9.7**. A variable attenuator, consisting of a half-wave plate and a PBS allows for the variation of single-pulse energy, and hence, bunch charge. A ground finished glass plate placed in front of a photodiode record the beam intensity and allow the adjustment of the variable attenuator to the desired level. The unpicked beam is rejected into a water-cooled beam dump.

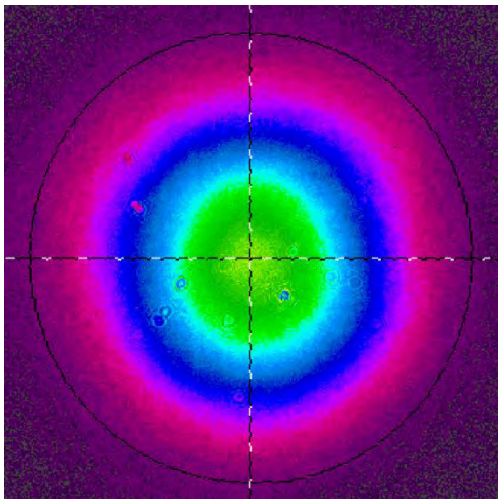

Figure 9.3. Transverse profile of the amplified beam, core is nearly Gaussian. [[9.41]; Courtesy of Lumera Laser GmbH]

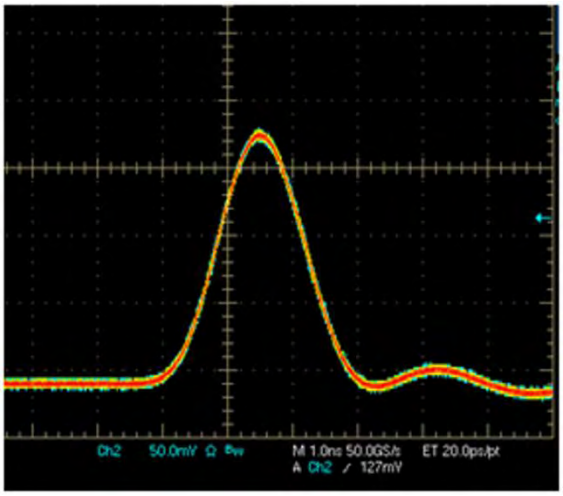

Figure 9.4. IR energy stability. Contrast is better than 1/1800. [[9.41]; Courtesy of Lumera Laser GmbH]

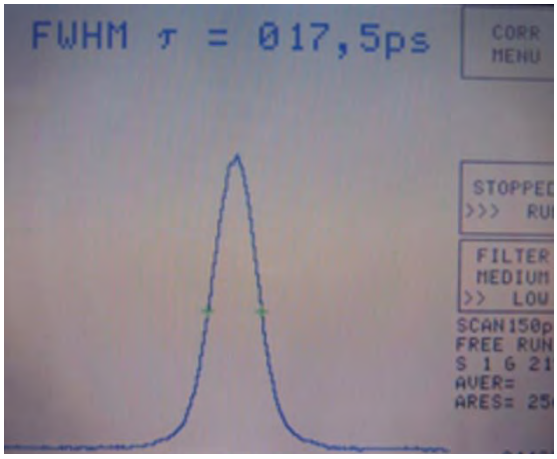

Figure 9.5. Pulse duration of the IR beam, 12 ps FWHM. [[9.41]; Courtesy of Lumera Laser GmbH]

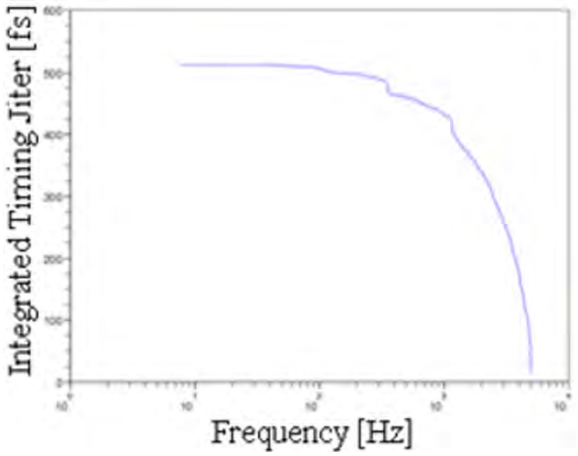

Figure 9.6. Jitter of the IR beam with respect to the master clock. [[9.41]; Courtesy of Lumera Laser GmbH]

9.3.4 Harmonic Crystals

The fundamental 1.064 μm radiation is first converted into 0.532 μm then 0.355 μm by harmonic crystals. The second harmonic crystal is a non-critically phase-matched LBO crystal maintained at 150 ˚C. A vertically polarized beam at 1.064 μm, focused to a beam waist of ~300 μm, is converted to a horizontally polarized 0.532 μm radiation with 50% efficiency. The transverse profile of this second harmonic beam is near Gaussian and the pulse duration is 8.2 ps. The residual 1.064 μm and 0.532 μm beams are re-collimated by an AR-coated achromatic lens for the subsequent third harmonic generation. If needed, the 0.532 μm beam can be separated from the fundamental by a dichroic mirror to exit the laser.

The third harmonic crystal is also a non-critically phase-matched LBO crystal maintained at 40 ˚C. The vertically polarized 1.064 μm and the horizontally polarized 0.532 μm radiation, are both focused down to a beam waist of 300 μm delivering vertically polarized 0.355 μm beam with an average power of ~5 W. The UV beam is separated by a series of dichroic mirrors and re-collimated to exit the laser. Leakage light from a Brewster window in the beam's path is used to monitor the UV power. Since the spot size in the crystal is small and both the average- and peak-powers are high, there is a very high probability of UV-induced surface degradation leading to damage to the harmonic crystals.

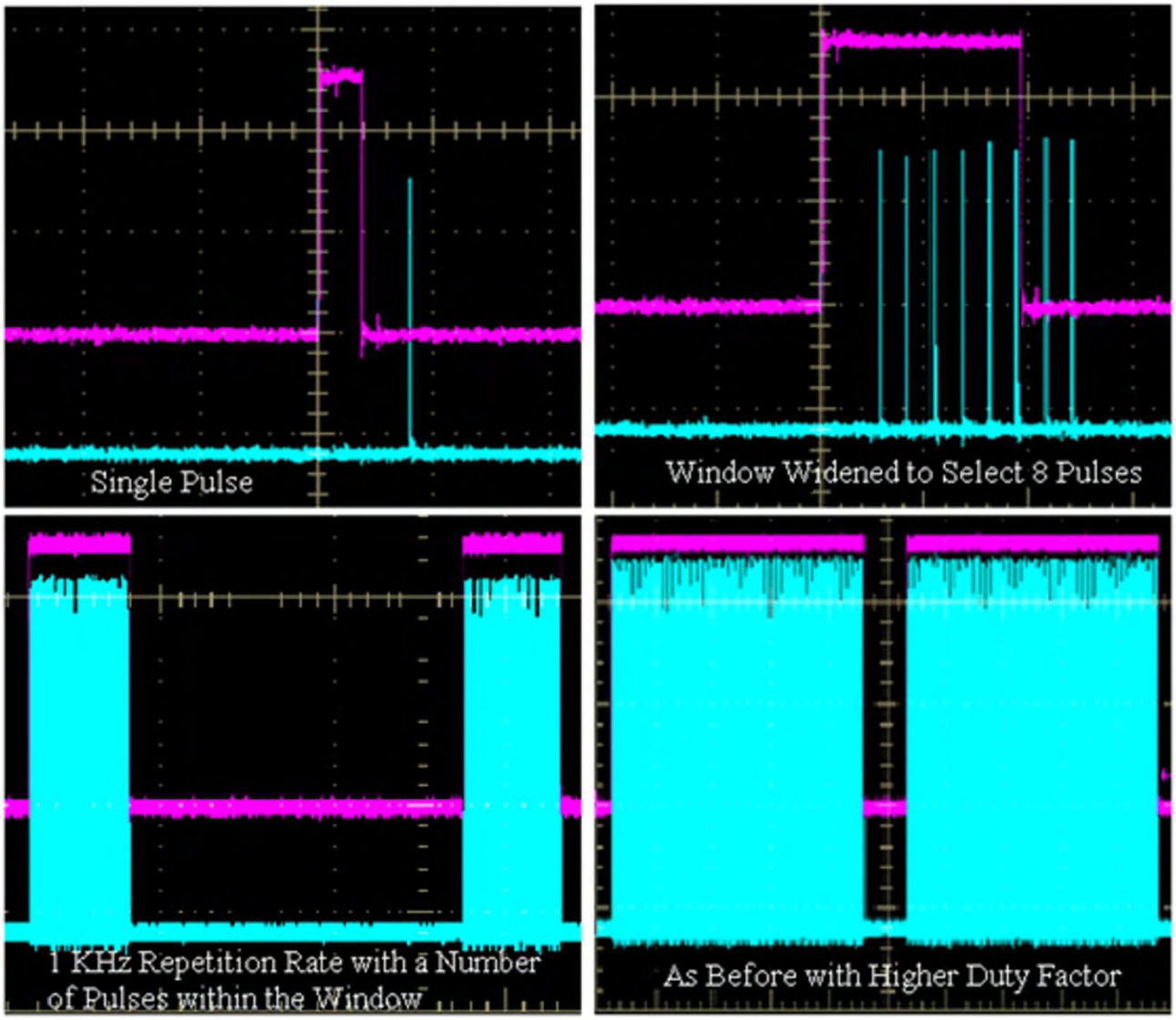

Figure 9.7. Different configurations of pulses from the pulse picker: Single micropulse, multiple micropulses, 1 KHz macropulse with varying number of micropulses within the macropulse envelop. Magenta lines indicate the shape of the high voltage pulse. [[9.41]; Courtesy of Lumera Laser GmbH]

The UV module is purged constantly with hydrocarbon-free air to increase the lifespan of the optical components and coatings. Furthermore, transversely oversized crystals mounted on an X-Y translation stage is used to move the crystals to a fresh location in case of damage. The pointing stability of the beam was measured to be ~3 microradians over 2 hr, well within the required range for the application. The beam walk

off in the THG crystal causes the appearance of a halo in the transverse profile of the laser beam that must be filtered before it propagates to the photocathode.

Similar Nd based systems are used in a number of facilities including DESY [9.42], [9.43], the Accelerator Test Facility at BNL [9.44], JLab [9.45], SPring-8 [9.46] and Boeing [9.5] to drive different photocathodes.

9.4 BULK SOLID STATE LASER SYSTEMS: $\lambda < 1$ μm

9.4.1 Ti:sapphire Laser

Ever since Moulton's pioneering work on Ti:sapphire crystal (Ti^{3+}:Al_2O_3) [9.47] in the 1980s and the discovery of a robust, passive Kerr-lens mode-locking mechanism [9.48], [9.49] in the '90s, femtosecond Ti:sapphire lasers became the work-horse of nearly all ultrafast laser applications. The superb physical properties of Ti:sapphire and technological advances in optics led to its dominance in the ultrafast laser field. Table **9.2** lists some important properties of this gain medium. The high thermal conductivity of Ti:sapphire requires minimal to no cooling. The long fluorescence lifetime of 3.2 μs allows multiple passes assuring efficient photon amplification and energy extraction. The mature crystal-growth technology affords superior optical quality Ti:sapphire crystals up to tens of centimeters in diameter. Ti:sapphire has a low parasitic absorption at its lasing wavelengths, and a large absorption cross section of ~4×10^{-19} cm^2 at 450-550 nm wavelengths (peak at 490 nm), resulting in a figure-of-merit greater than 200. This is the ratio of the absorbance at the peak absorption wavelength of 490 nm to that of the lasing wavelength, ($\alpha_{490nm}/\alpha_{800nm}$). Its exceptionally broad emission bandwidth of 660-1200 nm can support optical-pulse duration of just a couple femtoseconds (Figure **9.8**). With the invention of all chirped and double-chirped dispersion-control mirrors, a few femtosecond-long optical pulse with octave spanning spectrum is readily achieved, with superb stability over long term continuous operation. The broad bandwidth associated with such short pulse require careful selection of optical components, to compensate dispersion effects pertaining not only to low order terms, but higher order (up to fifth) terms as well.

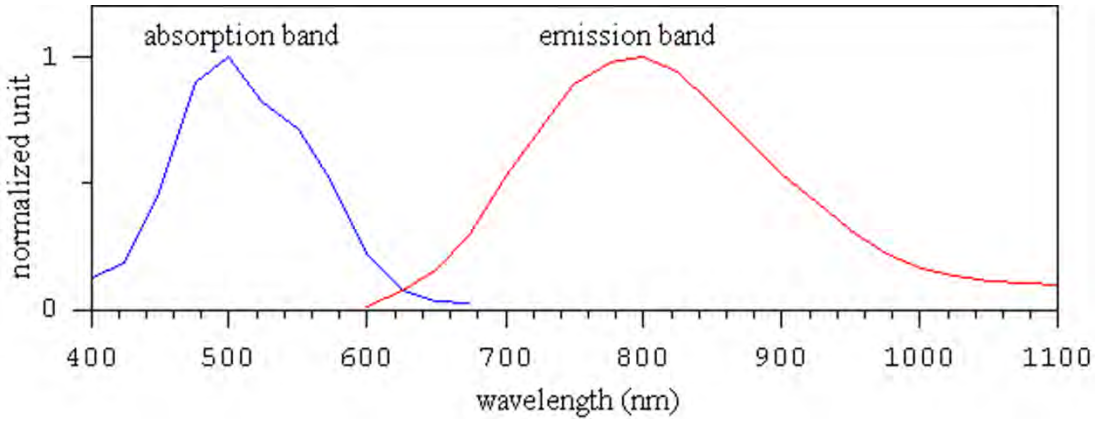

Figure 9.8. The absorption and emission spectrum of a typical Ti:sapphire crystal.

Such short laser pulses are advantageous in photoinjectors. As described in Chapter 1, electron beams with very small aspect ratio (ratio of longitudinal- to transverse-dimensions) emitted from the cathode will evolve under the RF field to have very small emittance. Such a beam requires a prompt photocathode and an ultrashort laser pulse, similar to that from the Ti:sapphire laser. Cathodes operating in multi-photon photoemission mode also would benefit from ultrashort, high intensity laser pulses on the cathode. Such an ultrashort pulse can provide sufficiently high peak power at energies well below the cathode's damage threshold. Furthermore, the photon energy of the doubled and tripled frequencies of Ti:sapphire laser is slightly above the work function of typical cathode materials used in photoinjectors. Thus, mode-locked

Ti:sapphire lasers are ideal to serve cathodes operating in both linear- and nonlinear-photoemission modes. Furthermore, using a single ultrafast Ti:sapphire laser to perform high resolution pump-probe experiments, such as electron pump and photon probe in ultrafast pulse radiolysis [9.50] and temporal electron bunch length characterization [9.51], photon pump and electron probe in ultrafast electron diffraction and electron microscopy [9.52], are very attractive because of the well-synchronized, short-pulse duration pump and probe.

9.4.2 Oscillator

In early days of femtosecond Ti:sapphire laser, oscillators were pumped by 5-10 W argon-ion lasers. Today, the 1-10 W diode-pumped, intracavity-frequency-doubled Nd:YVO_4 laser is the most preferred pump. As in Nd based systems, the cavity length of a femtosecond Ti:sapphire laser oscillator is adjusted to run at the n^{th} sub-harmonic of a reference RF frequency relevant to the accelerator. Ti:sapphire lasers are mode-locked to deliver a train of ultrashort pulses. Mode-locking can be initiated in a prism-pair, dispersion-controlled Ti:sapphire laser oscillator without a saturable absorber (schematically shown in Figure **9.9**) by simply taping on one of the cavity mirrors. Such passive mode-locking techniques include using a hard aperture Kerr-lens and saturable absorber mirrors. Active mode-locking, using acoustic-optical (A-O) modulators, supports phase-locking to an external RF source. As in Nd laser systems, to preserve phase-locking, the repetition frequency is monitored and the cavity length adjusted accordingly.

As seen from Figure **9.9**, using a fused silica prism-pair readily assures the generation of 10-20 fs light pulses. In this design, a thin gain crystal with a high FOM is used to eliminate the residual third-order dispersion in the cavity and to minimize the fifth-order while preserving a high gain.

The invention of all chirped and double-chirped dispersion control mirrors has significantly changed the Ti:sapphire laser oscillator, see Figure **9.10**. Although the chirped mirror design lacks the wavelength tuning capability and relies on a mechanical device to initiate its mode-locking, octave spanning spectrum is readily achieved with good long term stability. However, they are generally not used in photoinjectors because of space charge limitations; rather an intentionally frequency chirped, longer light pulse is used to mitigate the space charge effects. An oscillator emits an average optical power of 0.3-2 W at the center wavelength at 800 nm with spectral bandwidth of 20-90 nm depending on configurations. However, it emits only 2-4 nJ of energy per pulse, *viz.*, insufficient for most photoinjectors. The transverse beam profile of femtosecond Ti:sapphire lasers often are slightly elliptical, not Gaussian. This can be corrected in the final amplified beam by implementing a well-tuned amplifier cavity, to result in a high quality TEM_{00} Gaussian profile.

9.4.3 Pulse Stretcher and Power Amplifier

The output energy per pulse of a Ti:sapphire laser oscillator alone is generally not sufficient to deliver the nanocoulomb level charges needed for a photoinjector. Therefore, a laser amplifier or a series of power amplifiers normally are needed to boost the energy output of the oscillator.

The choices for amplifier configurations are regenerative- and multi-pass-amplifiers. In both schemes, to combat the self-focusing of a high peak power laser pulse in the gain medium that would lead to damage, the amplified pulse first is temporally stretched before amplification to reduce the peak power and recompressed afterwards, see Figure **9.11**, based on the chirp-pulse amplification technology developed by Strickland and Mourou [9.33].

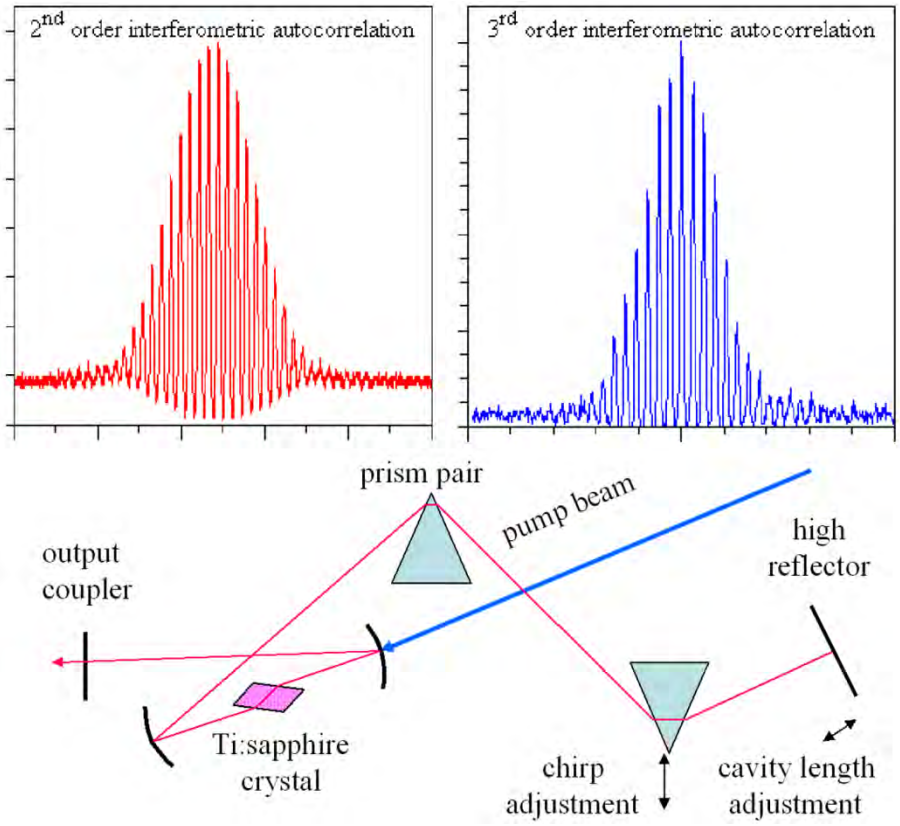

Figure 9.9. Layout of a conventional prism dispersion-controlled, mode-locked femtosecond Ti:sapphire laser oscillator and a typical 2nd and 3rd order interferometric autocorrelation trace utilizing, respectively, the 2-photon photoconductivity of a GaP diode, and the third-harmonic generation at the air-glass interface of a piece of 16 μm thick cover glass, $\Delta t \sim 15$ fs. The time axis of all interferometric signals is dictated by the fringe spacing, equals to an optical light field cycle; depicted is a 2.67 fs signal here at the carrier wavelength of 800 nm. [[9.53] (© 2005 Optical Society of America)]

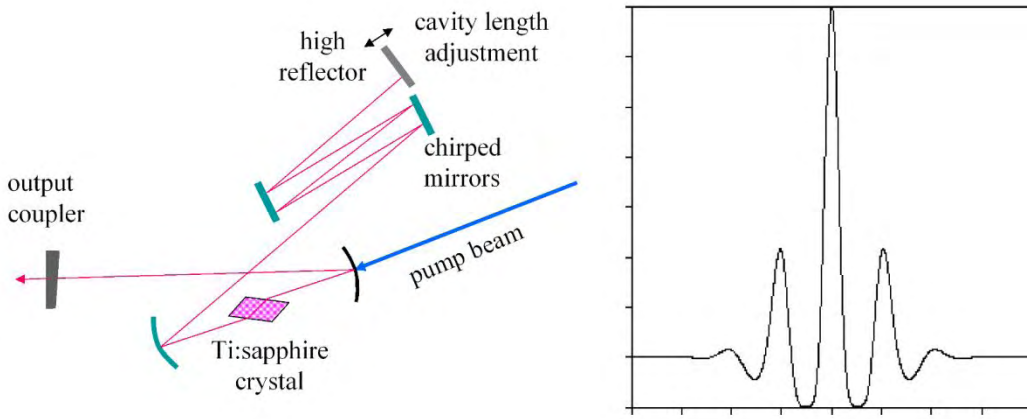

Figure 9.10. Layout of all-chirped mirror, mode-locked femtosecond Ti:sapphire laser oscillator and a theoretical 5 fs light pulse.

Although the simple Martinez [9.54] and Treacy [9.55] compression scheme was adequate to compensate picosecond light pulses, the ultrabroad bandwidth of femtosecond light pulse demands a simple, but quintic-phase-limited, aberration-free, chirped-pulse amplification system. However, the principle of chirp pulse amplification remains the same, where the ultrabroad bandwidth of a femtosecond optical pulse is first down-chirped using an optical stretcher and the chirped spectral components is then re-phased by a compressor. For temporal stretching, the all-reflective Offner stretcher design [9.56], [9.57] is preferred

because of its compactness, simplicity and high performance in ultra-broadband light pulse operation. In temporal compression, grating pairs are still the only available optics that can compensate large amounts of group velocity delay dispersion with high transmission efficiency and wide tunability. Using a careful alignment procedure [9.58], a dual grating pair can reliably compress the ultrabroad bandwidth femtosecond light pulse to its Fourier transform-limited pulse width.

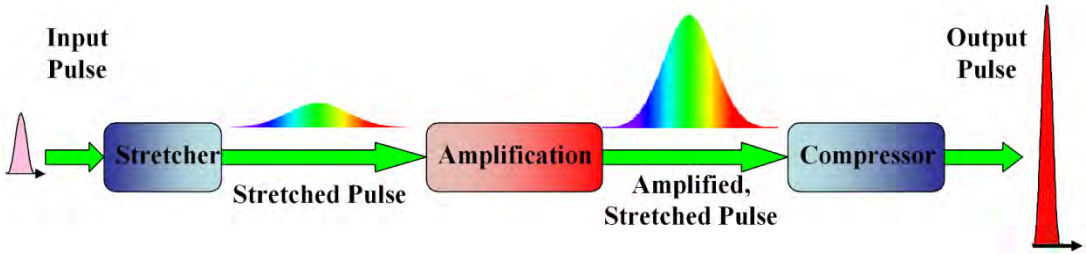

Figure 9.11. Conceptual illustration of laser chirped pulse amplification.

The first stage of the amplifier almost exclusively is a regenerative amplifier because of the maturity of the technology. Figure **9.12** is a generic layout of a regenerative amplifier. Although the output of a ~100 MHz repetition rate, femtosecond Ti:sapphire laser can exceed 1 W average power, usually 100-300 mW suffices for injection to a regenerative amplifier. In contrast, higher seed power is preferred in a multi-pass amplifier configuration.

Peak powers of terawatts at low repetition rates and average powers of hundreds of watts at ~100 MHz commonly are available in DPSS systems. New developments, such as cryogenically cooled DPSS systems are in the research and development stage and may be available within a decade.

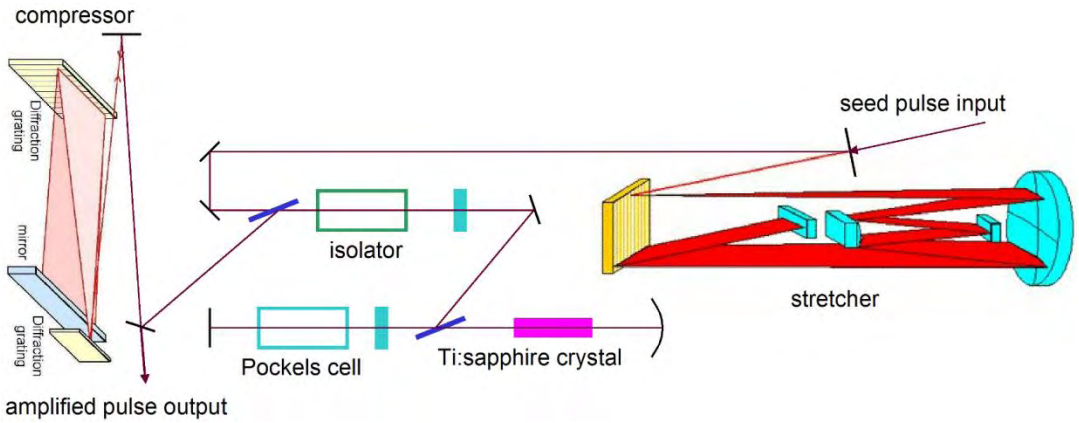

Figure 9.12. Typical regenerative amplifier arrangement, employing an all-reflective Offner stretcher and a pair of grating compressor.

The output power of the system can be increased by staging a series of amplifiers. The maximum power obtainable is limited by the components' damage threshold, the thermal effects, pump-power limitation and the required S/N ratio.

9.4.4 Harmonic Generation

Frequency up-conversion of the laser wavelength is accomplished by passing the high intensity laser beam through a nonlinear medium. The dipole moment induced by the laser field in the crystal contains the response of the crystal at both the fundamental and harmonic frequencies of the field. As each of these fields is described by their wave vectors, $k_{fundamental}$ and $k_{harmonic}$, constructive interference between the generated harmonic radiation will occur only if $(n_{fundamental} * \omega_{fundamental}) = (n_{harmonic} * \omega_{harmonic})$, where n and ω are the

refractive index and angular frequency, respectively. This condition is known as the phase matching condition. Since the refractive index in a birefringent crystal depends on the polarization of the light and the angle of incidence, one technique used in phase matching, known as angle tuning, is to select these two parameters appropriately for the fundamental and the harmonic frequency so that the phase matching condition is met over the entire length of the crystal. However, the broad bandwidth of the ultrashort laser pulses make it difficult to phase match the entire bandwidth over the full length of the crystal. Several techniques have been suggested for optimal phase matching over this large bandwidth [9.59]–[9.61].

The approach that has been used in some photoinjectors is using a thin crystal to minimize the walk-off, although this compromises the efficiency of the conversion process. LBO, BBO and KDP crystals are the most common materials for frequency doubling an ultrashort pulse of a Ti:sapphire laser because they can be phase matched over its entire tuning range and have low absorption both at the fundamental and second harmonic frequency. In selecting the crystal and the focusing geometry, care must be taken to evaluate the conversion efficiency, walk-off angle and damage threshold. Appropriate operating temperature and dimensions of the crystal, angle of incidence, divergence and the focal spot size of the laser must be determined. For high repetition rate lasers, the damage threshold due to the high average power should also be taken into account.

Figure **9.13** is a schematic of the Ti:sapphire laser system used at the LCLS; details and performance specifications are given in [9.62]. This well-characterized system was used to drive an X-ray FEL photoinjector. One major accomplishment is the high level of synchronization achievable between the laser, the electron beam and the user equipment. With a fiber-link system for distributing RF signals for the laser, a locking stability of 25 fs was attained between the reference and the laser [9.63]. Similar systems were used in SparC [9.64], SPring8 [9.65] and UCLA [9.66].

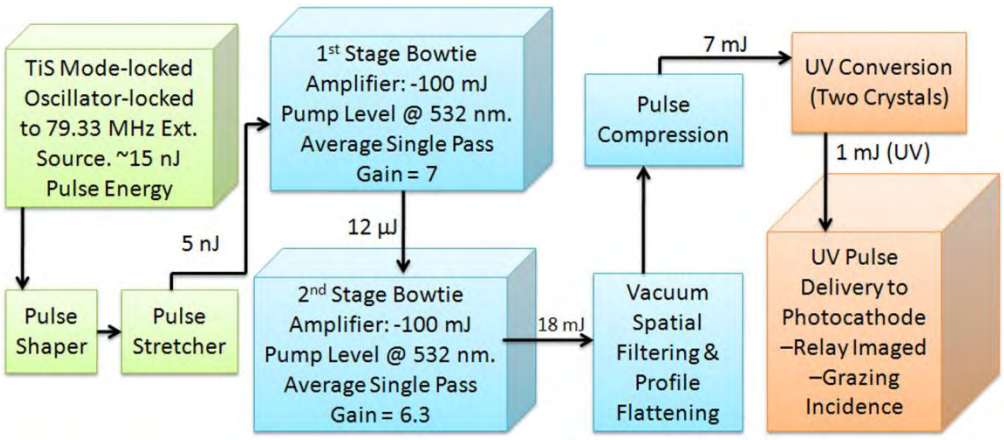

Figure 9.13. Schematic of the LCLS Ti:sapphire laser system.

9.5 FIBER LASER

The performance of fiber lasers has improved considerably in the past decade. This progress prompted their inclusion in this chapter, although their use in photoinjectors is not yet prevalent. As described earlier, laser beams with high peak power and high brightness were realized with diode-pumped, rare-earth doped, solid-state lasers. Typically, the gain medium is in the form of a rod. However, as pump power increases, the large energy difference between the absorbed and emitted photons elevated the heat load inside the gain medium. This power-dependent thermal distribution causes thermal lensing and heat-induced mechanical stress, leading to poor beam quality. Since fiber has a large surface area-to-volume ratio, heat dissipation in

this medium is significantly easier than in BSS lasers. Furthermore, since the laser radiation is confined to the waveguide structure of the fiber, the lasing occurs naturally in the mode supported by the fiber. Hence, the beam quality depends primarily on the design of the fiber.

An optical fiber consists of a core surrounded by cladding. The refractive index of the cladding is chosen to be smaller than that of the core so that the total internal reflection guides the optical beam within the core. If the core supports only a single mode (the chosen mode will have very low loss and the others will experience high loss), then only this preferred mode will propagate. In a typical single-mode fiber, the dominant mode is TEM_{00} and the beam's transverse profile is Gaussian. The most common gain media are different types of glass doped with rare-earth ions, Nd, Yb, or Er ions. Nd fiber lasers operate typically at 1.06 μm, while the tunability of a Yb fiber laser ranges from 1.03-1.1 μm [9.67]; that of an Er fiber ranges from 1.48-1.62 μm [9.68]. Fibers with dopants, such as praseodymium (Pr) and thulium (Tm), reach 2-3 μm wavelengths. Figure **9.14** is a schematic of the simplest form of a fiber laser [9.69].

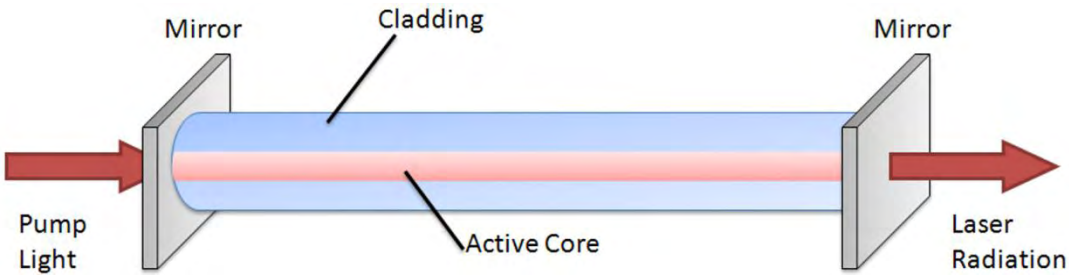

Figure 9.14. Schematic of the simplest form of a fiber laser. Both the pump light and the laser radiation are guided through its core. [[9.69] (© 2010 Optical Society of America)]

In a single-clad fiber, both the radiation from the pump and the laser are guided through the core. Since the core of a single mode fiber is typically in tens of micrometers, the output power is limited by the pump power that can be coupled into the fiber and the laser power that can be extracted without damaging the fiber. In this simple approach, the pump light must be of high mode quality for good coupling into the fiber. In pulse mode operation, the peak intensity of the laser radiation may be high enough to introduce nonlinear effects, such as self-phase modulation, four-wave mixing, self-focusing, and Raman and Brillouin scattering that should be avoided.

To increase the pump power and coupling efficiency, double-clad fibers with different inner cladding shapes were developed. Here, the core operates in single mode for laser radiation, while the inner cladding supports multimodes for launching the pump beam. Absorption efficiencies over 70% were achieved by optimizing the shape of the inner cladding and the position of the core within the inner cladding [9.70], [9.71].

For high-power operation, the core's mode volume must be increased without compromising the mode quality. The approach is to coil [9.72] a large mode area (LMA) fiber to increase the losses in the higher order modes, use of using photonic crystal-fibers (PCF), or use of fiber tapering, Figure **9.15** illustrates a cross section of a state-of-the-art PCF [9.69]. The 80 μm diameter, Yb/Al co-doped, active core is surrounded by three rings of small air holes with a pitch of 13.3 μm and diameter-to-spacing ratio of ~0.1 forming a 200 μm diameter inner cladding. The inner cladding guides the pump wavelength while the air holes confine the radiation in the doped region. The inner cladding is surrounded by an air clad consisting of ninety silica bridges, 400 μm thick and 10 μm long; this assures a ~0.6 numerical aperture for efficiently launching 976 nm multimode pump radiation into the fiber. A 1.5 mm fused-silica outer cladding surrounds this inner structure preserving its straightness and reducing bend-induced losses. With similar PCF fiber

laser technology, but of different dimensions, 1.064 μm, 2 W, 10 ps, 80 MHz output from a laser oscillator was amplified to an average power of 48 W at a peak power of 60 kW in a near-diffraction-limited beam with 70% polarization extinction [9.73]. It was achieved by significantly reducing the nonlinearity induced in the fiber; this key impact paves the way for employing fiber lasers in high peak power applications.

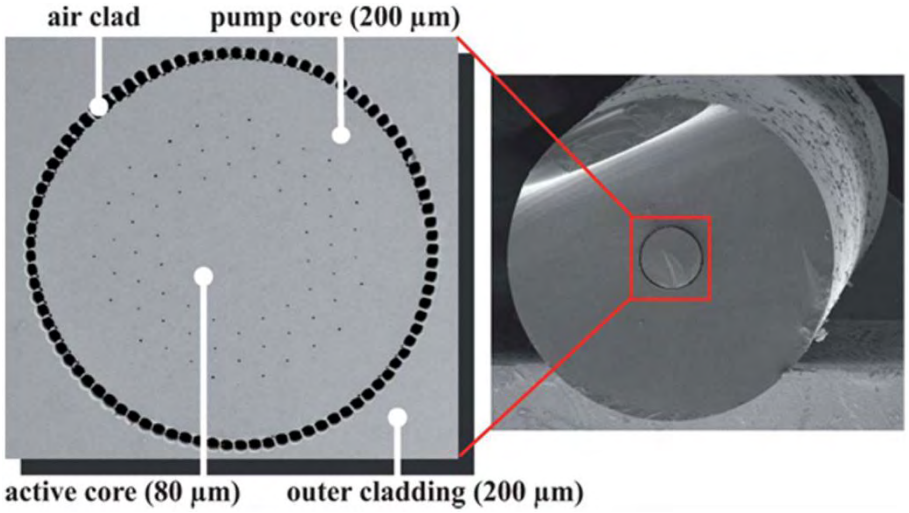

Figure 9.15. Cross sectional and expanded view of an LMA rod type PCF. [[9.69] (© 2010 Optical Society of America)]

However, at present only a few commercial fiber laser systems meet the specifications for the photoinjectors. However, there are several home-built [9.11], [9.74] and prototype [9.75] fiber lasers that meet the stringent photoinjector requirements. The design and operation of one of the prototypes is described below; this should be regarded only as a guideline because extensive research and development on high-power fiber lasers is ongoing.

9.5.1 Master Oscillator

A schematic of a fiber system is shown in Figure **9.16**. The compactness and the high efficiencies of fiber lasers make them attractive options for high repetition rate applications. The laser system can be an all fiber- or a hybrid-system. In the former, the oscillator also is a fiber laser, generating short laser pulses of low average- and peak-powers that are subsequently amplified. A number of techniques such as active mode-locking [9.76], passive soliton and saturable absorber mode-locking [9.77], [9.78] can produce ultrashort laser pulses from the fiber. Synchronization to the RF requires actively stabilizing the cavity length typically done by coiling the fiber in a cylindrical shaped expandable piezo drum.

Alternatively, in a hybrid system, electrically modulating the output from a semiconductor diode can supply the seed radiation for the fiber amplifier. This technique, as described in section 8.6 can be used to generate 30-50 ps laser pulses at 780 nm, with repetition rates ranging from 100 MHz to 3 GHz. Short pulse duration beam at desired pulse train mode can also be obtained by slicing the CW output of a diode laser with a fast electro-optic (E-O) amplitude modulator. A DC bias controller, superimposed with an impulse signal generated by a signal generator drives the modulator. By adjusting the amplitudes of the DC bias and the impulse signal, output pulses with duration of 50 ps can be generated. The repetition rate is varied by changing the pulse repetition rate of the signal generator. In the prototype system described in this section, the latter approach is adopted due to its simplicity.

In both of these approaches, the electronic control makes the synchronization to an external RF source relatively easy. However, the S/N of the output pulse, especially that of the E-O/A-O modulator, reaches

only ~10^4. This necessitates a smaller gain to be implemented on the subsequent amplifiers. This technique has been adapted to generate 1.06 μm radiation at a repetition rate of 700 MHz with a pulse duration of ~50 ps and single pulse energy of picojoules. Similar parameters at 1560 nm, which can be frequency up-converted after amplification for producing polarized electrons, can also be generated with this method.

9.5.2 Power Amplifier

The output power of fiber laser oscillator is typically insufficient for most photoinjectors; it is subsequently amplified in a series of fiber amplifiers. Power scaling in a fiber amplifier is limited by the onset of nonlinear effects and the maximum pump power that can be coupled into the fiber. The nonlinear effects include stimulated Raman scattering, stimulated Brillouin scattering and self-phase modulation. Although Watt to kilowatt high power pump diodes are commercially available, coupling such high power into micrometers to hundreds of micrometers diameter size optical fibers without encountering damage problems is still an issue, even for the large core fibers in millimeter diameter. Nonetheless, different techniques have been proposed to improve both the coupling efficiency and the out-coupled power [9.79], [9.80]. Using novel fiber coupling technique, multiple pump beams with a coupling efficiency of 67% into a final power amplifier, an amplified beam with up to 90 W at 1.06 μm, and 40 W at 0.532 μm, at ~50 ps pulse duration and 700 MHz repetition rate has been generated.

"Periodically poled nonlinear media" is the most preferred configuration for in-line harmonic generation where coupling from the amplifier to the nonlinear medium is straight forward and the conversion efficiency can typically reach > 70%. Even though the mode quality of the fundamental laser beam is TEM_{00} in both the transverse directions, the resulting harmonic beam typically is elliptical because of residual walk-off effects. Hence, care might be taken to re-shape the beam prior to irradiating the cathode.

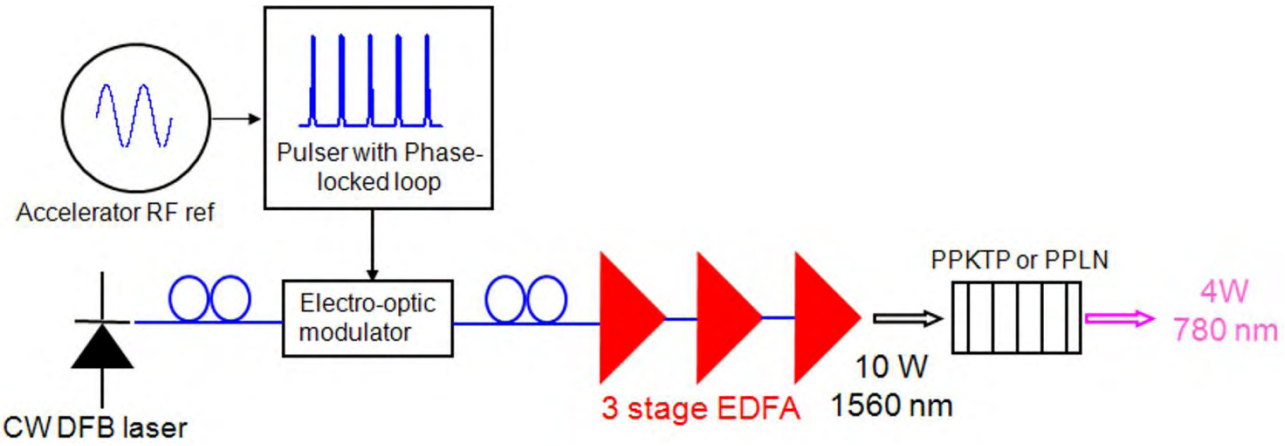

Figure 9.16. Schematic of hybrid system.

9.6 GENERAL CONSIDERATIONS

9.6.1 Beam Shaping (Transverse and Longitudinal)

As discussed in Chapter 1, various simulations [9.81], [9.82] suggest that modifying the transverse- and longitudinal-distribution of the electron beam from the nominal Gaussian to a beer can, an ellipsoidal, or a water-bag configuration (see Figure **9.17**), would lower the beam emittance [9.83]. As Luiten *et al.* demonstrated [9.84], when a 30 fs (pancake-shaped) electron beam of 100 pC charge from a 1 mm spot is launched into an RF accelerating field of 100 MV m^{-1}, the beam evolves into an ellipsoidal as it propagates through the RF injector. Their simulations revealed that, at a propagation distance of 200 mm, the emittance of the electron beam can be reduced from 3 μm for an initial Gaussian transverse-profile, to 1 μm for a flat-

top profile, and to 0.4 μm for an ellipsoidal profile. Such pancake beams were produced and propagated by shining a femtosecond laser pulse on metal photocathode (prompt emitter) in RF injectors [9.85].

Since the spatial- and temporal-profile of a laser pulse can be transferred simply on to the photo-ejected electrons with minimum distortion, shaping the driving laser beam to the desired three-dimensional profile may offer an alternative route to obtaining an electron beam with ultralow emittance. Schemes to obtain spatiotemporal flat-top laser pulses were demonstrated at SPring8 [9.86], DESY [9.87], LCLS [9.88], [9.7] and EUROFEL [9.89].

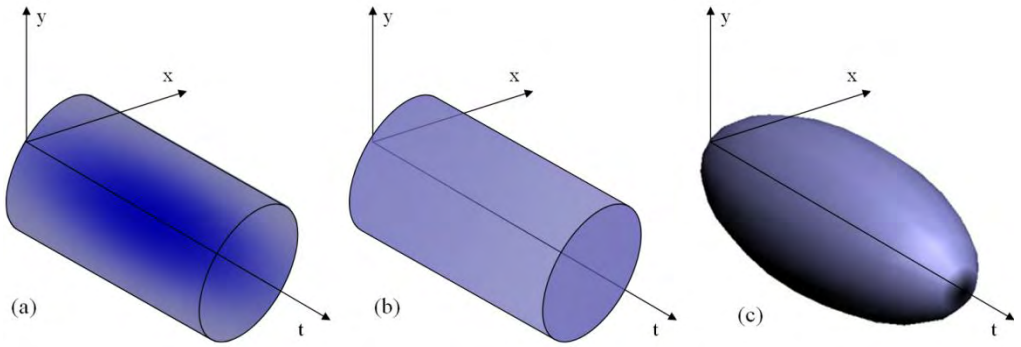

Figure 9.17. Spatiotemporal profile of (a) conventional Gaussian intensity-distribution with a fixed cylindrical cross section, (b) beer-can wherein the light intensity is constant over the entire cylindrical volume, and (c) 3-D uniform ellipsoidal, where the intensity is constant, but with a time-dependent spatial; *x* and *y* are the spatial coordinates and *t* is the time axis.

9.6.2 Temporal Shaping

The techniques used for temporal shaping depend strongly on the duration of the initial laser pulse. When laser pulses are longer than a nanosecond, they can be shaped directly by E-O modulators. These advanced modulators have tens of gigahertz speed [9.90]. Sub-picosecond and femtosecond light pulses intrinsically have large spectral bandwidth, and hence, they can be temporally shaped by modulating the laser pulse's spectral content. Weiner [9.91], who pioneered this approach, has extensively reviewed this technique.

Figure **9.18(a)** shows the basic principle of the process. A grating first disperses the frequency content of the laser pulse. The first Fourier lens transforms the angular dispersion from the grating to diffraction-limited spots at its focal plane, with well defined position to frequency correlation. Spatially patterned amplitude- and phase-masks manipulate the spectral content at this plane. A second lens-grating pair unfolds this modulated beam and recombines all frequency components into a single beam with a modulated temporal shape. For ideal shaping, the grating-lens combination without the mask must be dispersion free, that is, the output beams must be identical to the input when the phase mask is absent.

Using fixed amplitude- and phase-masks, 75 fs laser pulse at the wavelength of 0.62 μm was temporally shaped to ~2 ps pulse with rise and fall times of ~100 fs [9.92]. Employing a mechanical aperture of adjustable size, flat top UV pulses of ~8 ps FWHM were obtained from a 100 fs Ti:sapphire oscillator-amplifier system [9.93]. The major advantage of such static mask modulators is the ease of their fabrication and simplicity of the overall system. However, fabrication cannot be undertaken without a complete knowledge of the input pulse. Therefore, different masks must be designed, inserted, and aligned for different pulse shapes.

Temporal shape can be controlled actively by replacing the fixed mask with programmable liquid-crystal-spatial-light-modulator (LC-SLM), movable mirror, deformable mirror, or an A-O modulator. High quality

square pulses were generated by modulating the spectrum of a 50 fs pulse from a Ti:sapphire laser with a computer-controllable SLM; a reduction in the beam emittance of a photoinjector was observed [9.94]. In that work, a LC-SLM with 128 pixels served as the phase mask and the period of the pixels was 100 μm with a 3 μm transparent gap between electrodes. The resolution of the phase shift on the LC-SLM was ~0.01π. Positioning this pulse shaper between the oscillator and the pulse stretcher lowered the likelihood of damaging the pulse shaping optics. The transmission of the laser power through the pulse shaper was about 60%. Using this device, the authors have compared the emittance of 0.6 nC beam with 9 ps FWHM Gaussian and square pulse shapes in the longitudinal dimension. Normalized emittance of $1.38 \pm 0.06\,\pi$ mm-mrad and $0.95 \pm 0.03\,\pi$ mm-mrad were obtained for the Gaussian and square shapes respectively, resulting in ~ 45% improvement in the emittance. The optimal bunch length for this charge was found to be in the range of 8-9 ps. Since the optimal bunch length depends strongly on the charge, current density, accelerating field and RF phase, this optimization needs to be executed for the parameters of interest.

A-O modulators with a programmable dispersive filter (commercially known as DAZZLER) have successfully shaped [9.95]–[9.97] picosecond- and femtosecond-pulses (see Figure **9.18(b)**). Employing a DAZZLER to shape the IR beam to a 15 ps long rectangular profile followed by frequency tripling to the UV, a 17-25% reduction in electron beam emittance was observed [9.97]. Although these active pulse-shaping techniques are well developed, powerful, and can deliver arbitrary temporal pulse shapes, they have limitations, *viz.*, their low optical-power handling capabilities make them applicable only to low repetition rates and the output may contain residual spatiotemporal distortions. Furthermore, very often only UV photons (the second-, third-, or fourth-harmonic of the light pulse) are sufficiently energetic to liberate electrons from a photocathode. Although it is highly desirable to shape the temporal pulse in the final UV pulses, the conventional SLMs do not function well at these short wavelengths. Recently, a UV version was introduced; its performance has not been thoroughly tested in these applications. If modulation is executed at the fundamental wavelength, then care must be taken so that no additional spatiotemporal distortions are introduced in the frequency-conversion process.

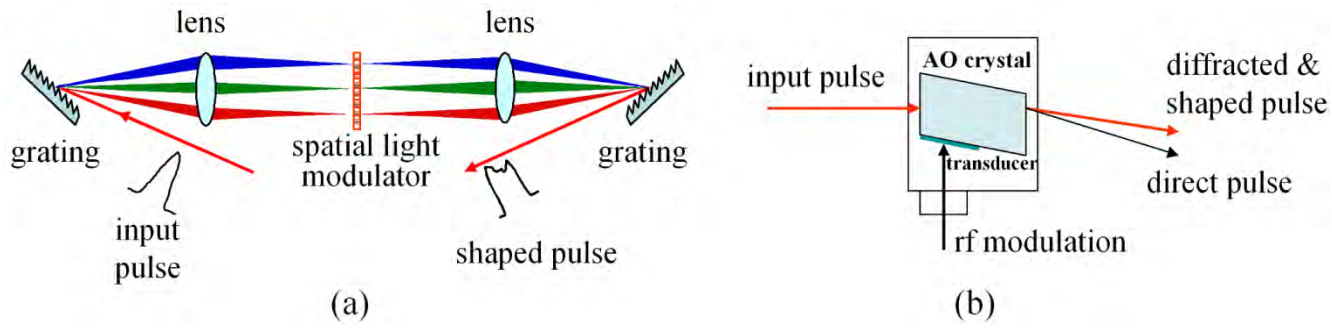

Figure 9.18. Conventional temporal shaping using, (a) Spatial Light Modulator, and (b) DAZZLER.

Alternatively, passive pulse stacking is commonly used to temporally shape energetic ultrashort laser pulses of hertz to megahertz repetition rate [9.98], [9.99]. This approach proved more successful with picosecond pulses wherein the spectral bandwidth is not large enough for accurate modulation in the spectral domain and the modulator's response time is not fast enough for modulation in the time domain. Such pulse stackers can be constructed either with a set of appropriately oriented birefringent crystals [9.100]–[9.102] or a conventional delay line [9.1], [9.103]. Both these passive techniques require precise interferometric alignment.

The conventional delay line consists of various optical elements to stack pulses in a cascading fashion. The number of optical elements required as well as the interferometric precision needed in pulse stacking greatly complicates the alignment and stabilization schemes to such a high precision.

With the birefringent crystal and a single polarized light pulse passes through a properly arranged birefringent crystal, the ordinary- and extraordinary-components of the light pulse propagate with different group velocities, resulting in a time-dependent change of polarization (Figure **9.19**). Coupling this output pulse with a polarizer splits the single input pulse into two output pulses, with the time delay between them dictated by the two refractive indices and the length of the crystal. The temporal pulse thus is stretched with a predetermined intensity modulation. Interferometric precision is achieved by accurately controlling the length of the crystal. This approach, which is relatively simple [9.101], results in stable pulse shape, but offers only limited control of the final pulse shape. Using a stack of three appropriately oriented YVO_4 birefringent crystals of thicknesses 24-, 12- and 6-mm respectively, a 10 ps laser beam at 532 nm was stretched to 60 ps [9.101]. The transmission efficiency of the arrangement is 62%, limited by the crystal's intrinsic absorption loss. Insertion loss can be lowered significantly by carefully selecting low absorption crystals.

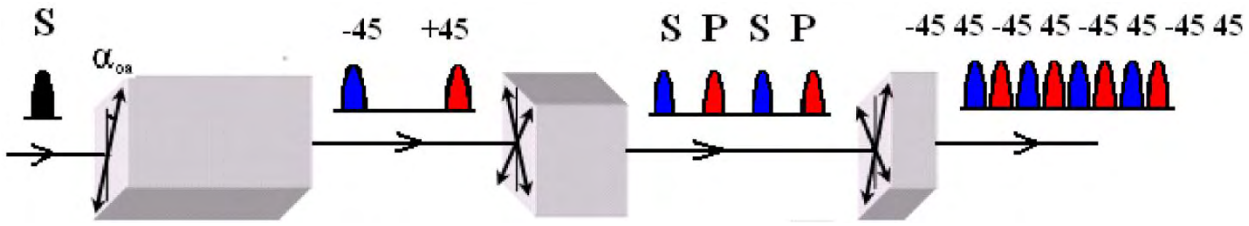

Figure 9.19. Passive pulse-shaping by cascading several birefringent crystals. The optic axes are shown by thin lines on the surface of the each crystal. The polarization of the laser pulse is depicted by thick double arrows in each crystal. An input S-polarized pulse first is split into two replicas with various amplitude and temporal delays along the ±45° of the crystal axis. Subsequent crystals are arranged with the optics axis rotated 45° with respect to the preceding one. In this manner, a stack of n birefringent crystals will generate 2n replica pulses. It is possible to generate arbitrarily shaped pulse controlling their relative temporal delay and amplitude. [Adapted figure with permission from [9.101]. Copyright 2009 by the American Physical Society]

9.6.3 Spatial Shaping

The conventional spatial beam shaping technique relies on imaging a predefined circular aperture using relay optics on to a photocathode. Although near flat-top profile can be achieved, the process introduces excessive optical loss with added risk of injecting airy fringe pattern onto the photocathode. Alternatively, the spatial profile may be shaped by controlling the optical transmission in the radial direction with either an inverse-Gaussian transmission filter [9.104], diffractive elements [9.105], [9.106], or by actively controlling the reflected/transmitted laser beams by controlling the mirror/lens in the beam path to produce the desired beam shape. Recently, commercial passive aspheric refractive/reflective optical shaping systems have become available [9.106]–[9.109]. They offer a robust yet simple design, with high optical transmission and high optical-power handling capability down to the UV wavelengths. Figure **9.20** depicts the ZEMAX simulated ray-diagram of the π-shaper (Newport Inc.), the simulated input- and output-beam profiles, and the experimental results [9.101]. With a Gaussian input-beam diameter of 4.7 mm, the π-shaper produces a high-quality flattop transverse profile with a diameter of 6.5 mm FWHM.

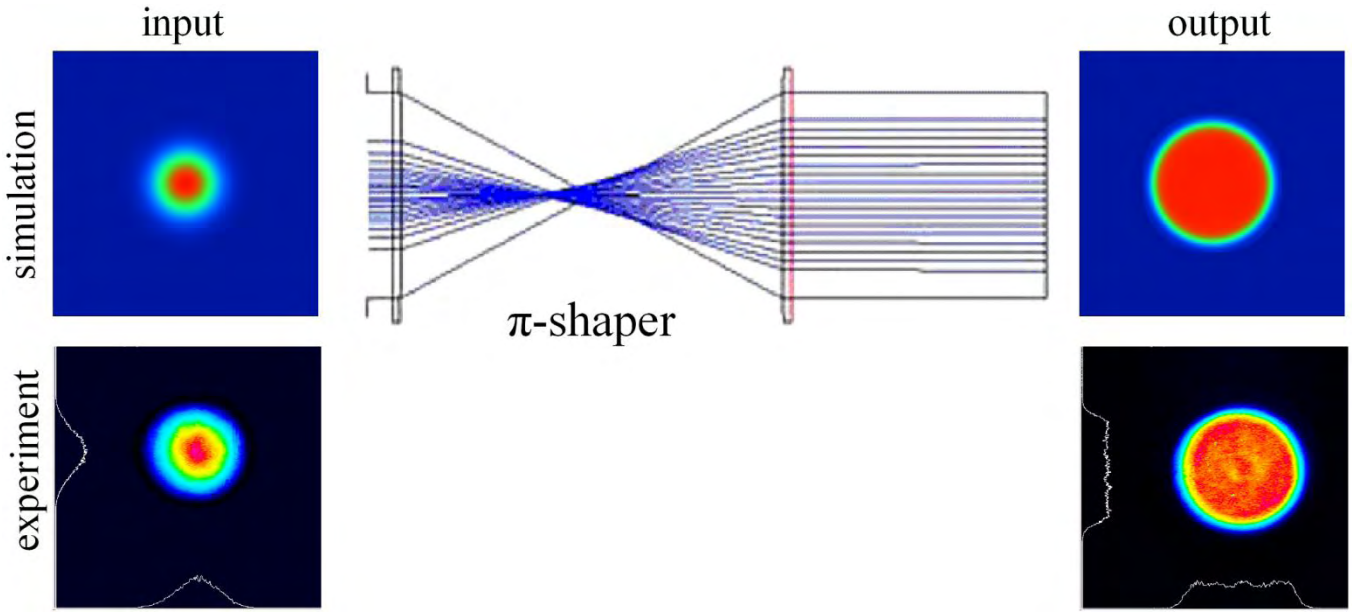

Figure 9.20. Passive spatial π-shaper. Top: ZEMAX simulation of transverse beam distribution modified from a Gaussian at the input end to a uniform cylindrical output profile using a π-shaper. Bottom: Experimental profiles of input- and output-beam. [Adapted figure with permission from [9.101]. Copyright 2009 by the American Physical Society]

The sensitivity of the π-shaper with respect to the angular misalignment (or tilt) and laser beam de-center (or beam lateral offset) was studied [9.101]. Using ZEMAX simulation it was shown and verified experimentally that the tolerance of this π-shaper is ±9 mrad in tilt angle and ±0.38 mm in de-center (Figure **9.21**). The experiment agrees well with the simulation. These tolerances also dictate the acceptable beam pointing error of an input laser beam.

The passive shapers are designed for specific beam-parameters, such as the size and divergence of the input and output spots; they work very well for Gaussian beams. Since both the position and angle of incidence could change due to pointing instability, the sensitivity of the beam shaper to misalignment is an important consideration in its design. Figure **9.21** illustrates the change in the beam profile due to shift in the location and angle of the centroid.

High-quality spatial profiles other than flat-top ones can be obtained with various optical-design modifications [9.110], [9.111]. A complete spatiotemporally shaped light pulse is generated by cascading a temporally shaped ultrafast light pulse followed by a spatial shaper.

Figure **9.22** illustrates the transverse- and longitudinal-beam profile of the beam [9.101] at different locations along the laser-beam transport that includes a pulse stacker and a π-shaper. The Gaussian transverse and temporal profile for the laser beam is depicted on the left side of the figure. Its flat-top profile obtained after passing through a beam stacker and a π-shaper near the laser is shown in the middle. The beam then is relay imaged onto the location of the photocathode ~9 m away from the laser. The flat-top image is a reproduced, with minor additional modulations, after the relay optics, shown on the right of Figure **9.22**. It was shown experimentally [9.100] that the electron beam profile mirrors that of the shaped laser beam.

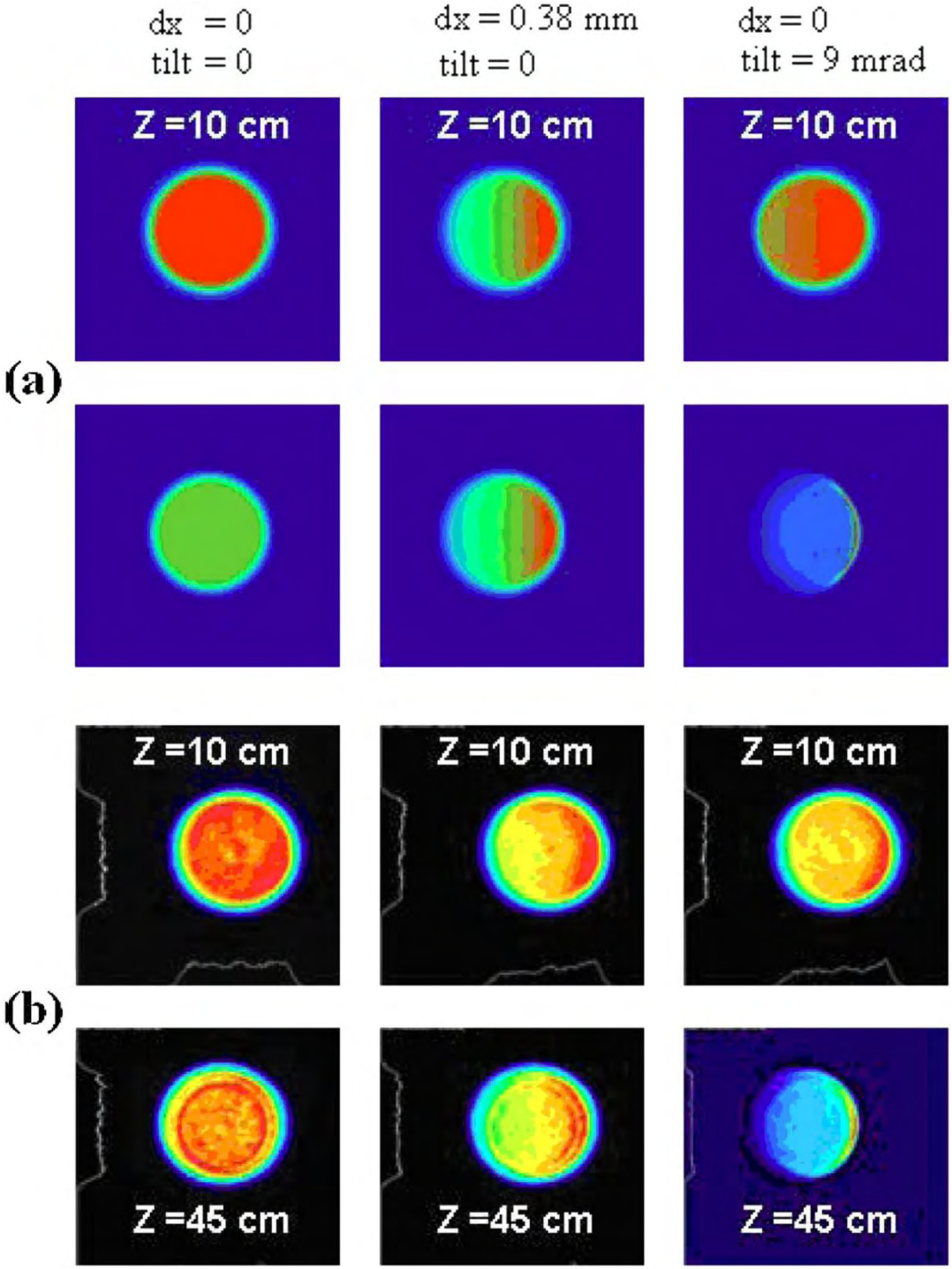

Figure 9.21. Spatial beam profile at 10- and 45-cm away from the π-shaper under different alignment conditions, illustrating its sensitivity to beam shift and tilt with respect to the optical axis: (a) ZEMAX simulation; (b) corresponding experimental profiles. [Reprinted figure with permission from [9.101]. Copyright 2009 by the American Physical Society]

The ellipsoidal profile is characterized with a constant energy density (thus, charge density) distribution at a given time slice, as shown in Figure **9.17(c)**. However, it displays a time-dependent change of beam size. This unique beam is characterized by spot size that is small at the beginning and the end of the pulse duration, but grows larger towards the middle. It is particularly challenging to generate such an ellipsoidal beam profile where the laser pulse must be shaped spatiotemporally in 3-D. Some suggested techniques use

adaptive 2-D deformable mirrors or 2-D spatial light modulators in combination with a temporal shaper [9.85]. Recently, an elegant solution was proposed that uses the unique properties of an ultrashort light pulse. The basic principle is as follows: the modulation on the instantaneous frequency of a light pulse leads to time-dependent phase changes. The chromatic aberration of a subsequent focusing optics, converts this shift of the instantaneous frequency ($\delta\omega$) to a change in the focusing length of a lens (δf)

$$\delta f = \frac{-f_0}{n_0 - 1}\frac{\delta n}{\delta \omega}\delta\omega \tag{9.1}$$

where f_0 and n_0 are the nominal focus length and refractive index of the lens. In this manner, a time-dependent frequency change is mapped into a time-dependent focal length (Figure **9.23**). A DAZZLER, most suitably, realizes these modulations because therein the amplitude and phase of a light pulse can be controlled arbitrarily. Figure **9.23** illustrates the experimental arrangement and some results have been obtained using this method [9.112]. However, not only is generating this ellipsoidal profile complex, considering the ultrashort time scale on the change in spot size, but confirming this time-dependent behavior of beam size is equally difficult.

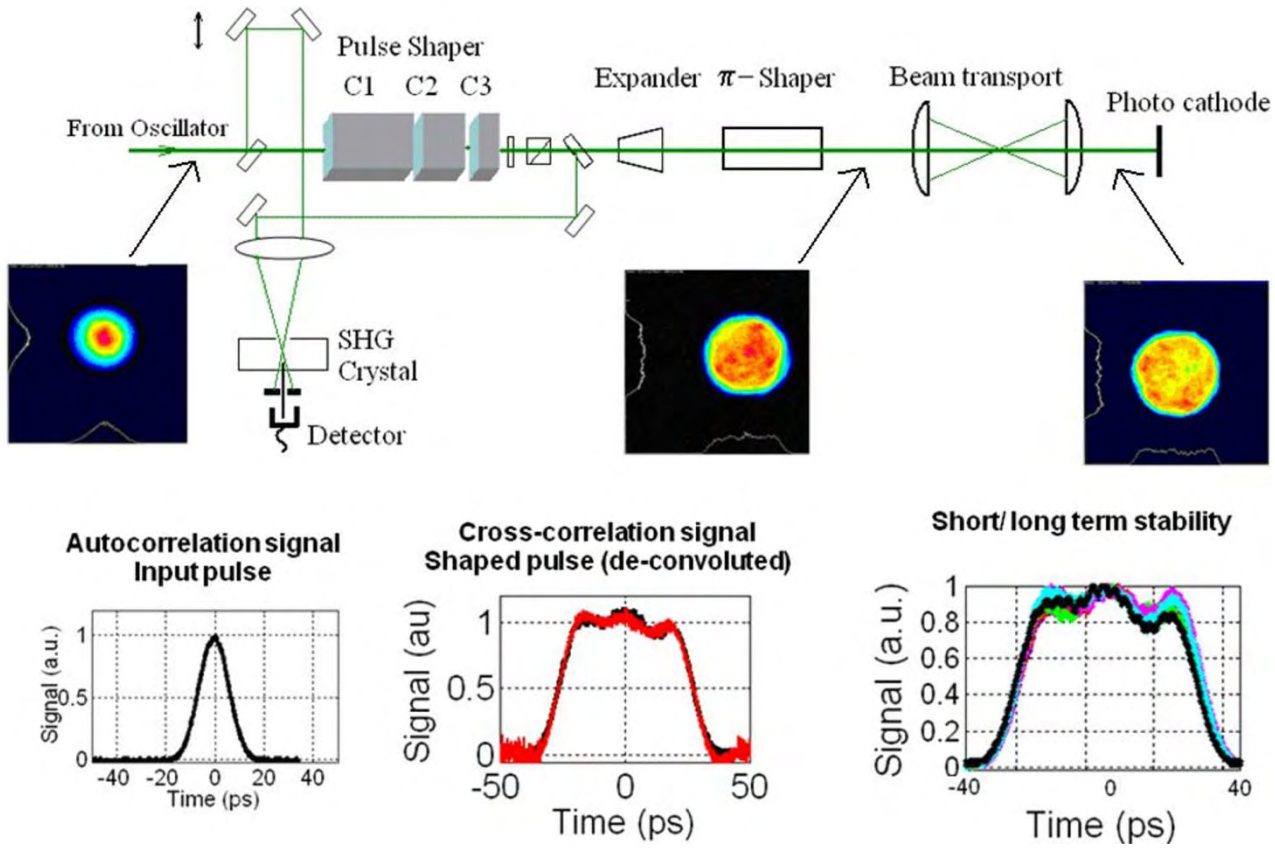

Figure 9.22. Spatial- and temporal-profile of the laser beam as it propagates along the beam transport. Left: Output of the laser; Middle: Spatially shaped by beam shaper and temporally shaped by beam stacker near the laser; Right: Shaped beam after relay imaging to the cathode location, 9 m away from the laser. [Adapted figures with permission from [9.101]. Copyright 2009 by the American Physical Society]

Despite the successful developments on spatiotemporal pulse-shaping techniques, they all have their advantages and disadvantages; and no one scheme suits all accelerator facilities. Indeed, spatiotemporal shaping is only the beginning in producing a low-emittance electron beam. Equal emphasis should be given

to transporting the electron beam to preserve its quality. A well-designed spatiotemporal shaper with proven robustness, combined with a feedback system based on the electron beam characteristics and a self-learning algorithm eventually should lead to the next generation of ultrahigh brightness electron beams.

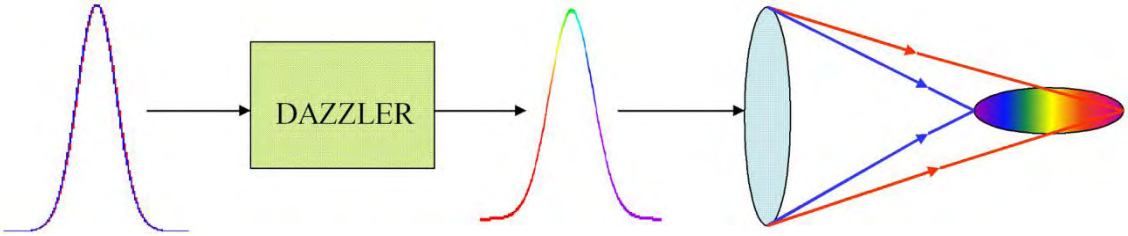

Figure 9.23. Simplified schematic of a time-dependent frequency pulse mapped onto a time-dependent focal length that can produce an ellipsoidal spatiotemporal profile in 3-D.

9.6.4 Beam Transport and Diagnostics

Preserving the beam profile as well as the timing synchronism is critical for generating reliable low emittance beams. It is a general practice to use low-dispersion vacuum windows, ultra-broadband silver- or gold-coated mirrors for low-power beams and ultra-broadband dielectric mirrors for high power beams. Typically the laser room is not in close proximity to the interaction region and the laser beam has to be transported over long distances with varying climate. Hence, careful design of the beam transport and monitoring the parameters are essential for reliable operation of the injector. Normally an overfilled iris or the image location of the spatial profiler is relay imaged on to the photocathode. It is beneficial to use a beam tracking code such as ZEMAX to trace the laser beam from start to finish and compare the results to the measurement for better understanding of the beam optics, especially when the beam is non-Gaussian. Enclosing the beam fully by evacuated pipes will minimize the climate related beam fluctuations. Use of remotely controlled mirrors, especially in high radiation area is necessary for online adjustment of the laser beam optics. Extensive use of irises and displays of beam position on these irises are recommended for correcting the beam path when needed. The laser energy, beam profile, location, pulse duration and timing should be monitored as much as possible and displayed in the laser room/control room to facilitate trouble shooting and correcting. Critical parameters should be displayed in the control room so that laser parameters can be correlated to electron beam parameters.

Other engineering aspects for the reliable and routine operation of all lasers, especially for photoinjectors are to hermetically enclose all oscillator components; temperature-stabilize the optical base plate containing all optics including the pump source; use low-profile optical mounts to minimize vibrations; minimize the distance between the pump and the gain crystal to reduce the effect of the beam pointing instability of the pump source; and, finally, regulate the temperature, cleanliness and humidity of laser room. All these parameters are paramount to a low (sub-100 fs) timing jitter needed for the photoinjector system.

9.6.5 Timing and Synchronization

Maintaining the frequency and phase relationship of the RF cavity in a photoinjector at all times is one of the most important parameters of an accelerator facility. An even more stringent requirement is that all the reference signals distributed throughout the facility should be synchronized accurately, since low-timing jitter leads to better experimental accuracy. Timing accuracy starts by examining the frequency stability of a high-precision, frequency synthesized RF clock, the repetition frequency of the laser oscillator and the transit time change for the reference signal. Assuming that the master clock determines the RF frequency and phase, we then look at other timing drifts. The cavity round-trip time, or the repetition rate, often drifts with time due to environmental disturbances, such as changes in temperature and acoustic noise. Likewise,

changes in the cables' lengths could introduce timing drifts in trigger signals. In general, the laser is phase-locked to the master oscillator, or its sub-harmonic, to maintain its synchronism. A typical phase-lock [9.113] loop, shown in Figure **9.24**, is used to lock an RF source to the repetition rate of the laser to provide accurate timing.

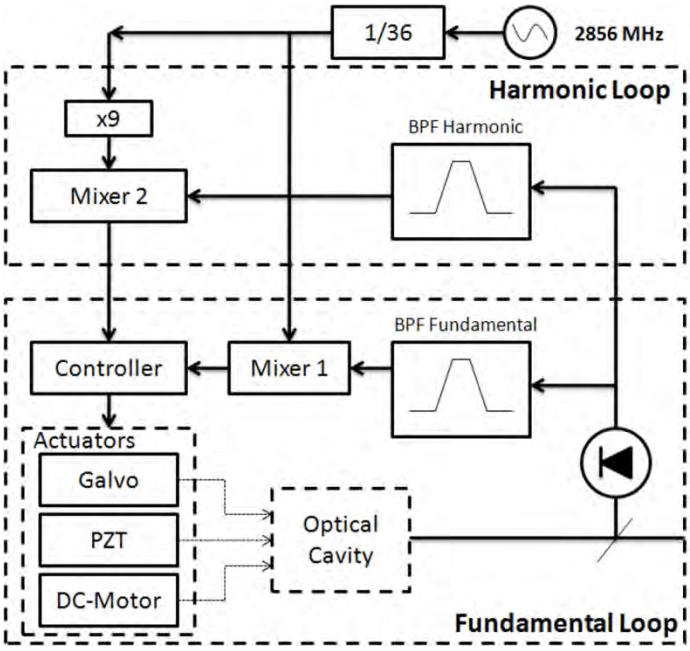

Figure 9.24. Signal from the master oscillator is compared to the signal in the mixer from the laser, and the error signal from the mixer is used as a feedback to adjust the laser cavity length. [9.113]

Phase-locking at the higher harmonics of an RF source would provide a better timing accuracy. As is evident from Figure **9.25**, the slope of the harmonics at zero crossing, depicted and highlighted, increases linearly with the harmonic number *n*, that is,

$$\left[\frac{\Delta V}{\Delta t}\right]_n > \left[\frac{\Delta V}{\Delta t}\right]_{n-1} \tag{9.2}$$

Therefore, a smaller Δt can be registered by the same ΔV at the higher harmonic. This ΔV often is used as a feedback signal to control the length of the oscillator cavity. In practice, reaching the higher RF harmonics at the equivalent RF power as the fundamental requires much RF power. Consequently, analog phase-locking electronics often lock only to the first few RF harmonics, but this is sufficient for the oscillator's output to reach 50 fs timing jitter. As shown in the Nd system in Figure **9.24**, two feedback loops generally are employed; a slow feedback loop (100 ms to tens of seconds) corrects time drift due mostly to the thermal environmental effects and a fast feedback loop (< 100 ms) corrects all other electronic time-drifts.

Von der Linde developed an approach to measure the time jitter of a mode-locked femtosecond laser oscillator into the femtosecond range [9.114]. This quantitative timing jitter is obtained first by measuring the RF spectral intensity of the n^{th}-harmonic of the laser's repetition rate, then by integrating the single sideband phase-noise from 0.1 Hz to 100 kHz from the n^{th}-harmonic of the laser's repetition rate (Figure **9.26**). Using this approach, a timing jitter approaching 10 fs was measured.

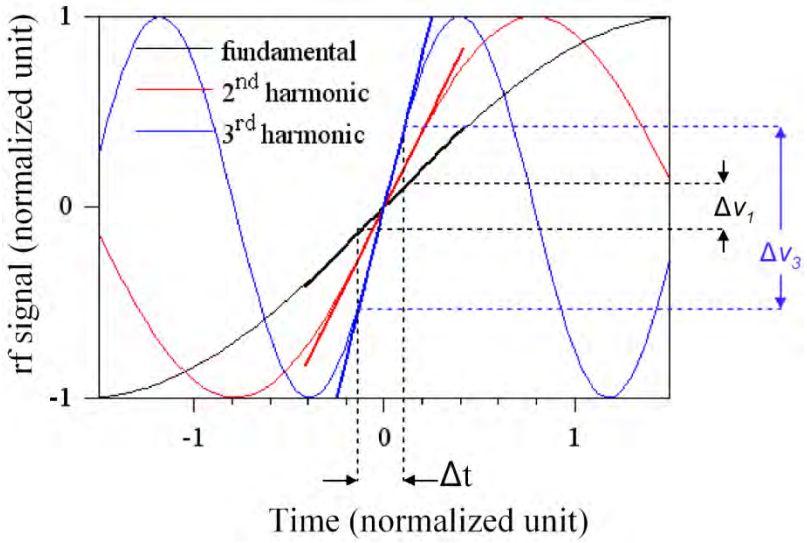

Figure 9.25. Improvement of sensitivity with higher RF harmonic signal. The slopes of the 1st, 2nd and 3rd harmonics are highlighted about time $\Delta t = 0$.

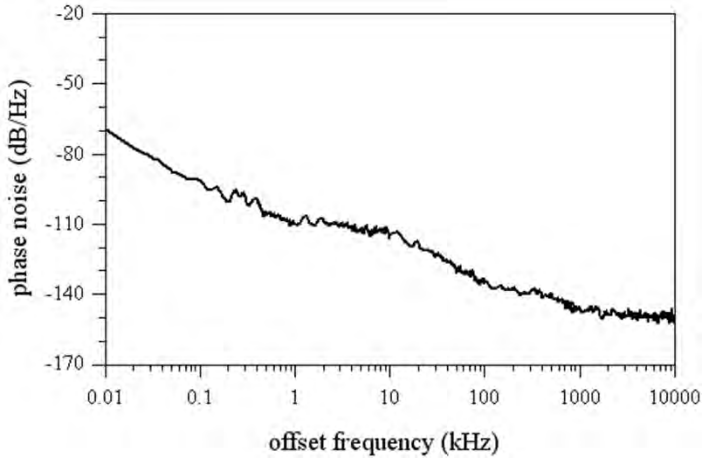

Figure 9.26. Representative trace of the spectral intensity of the n[th]-harmonic of the laser repetition rate of an RF oscillator.

Timing jitter does not degrade much when the seed pulse propagates through the chain of amplifiers operating in a stable environment. However, a larger timing jitter arises when the short laser pulse is delivered to different parts of a photoinjector facility that often are separated by 10-100 m and have large differences in temperature and environment. To deliver a femtosecond timing-link using a stabilized clock, Kärtner developed a bunch arrival time (BAT) fiber-link-timing synchronization unit [9.115]. It is a self-aligned, balanced, cross-correlator with no moving parts based on a type-II $KTiOPO_4$ optical-harmonic generation crystal, wherein an outgoing and a returned light pulse are cross-correlated through a long fiber link to generate a time-error signal and to close a feedback loop. Long-term timing stability reaching 10 fs precision has been established. These ultrastable timing levels of synchronization were achieved at LCLS after deploying these bunch arrival time (BAT) units.

9.7 CONFLICT OF INTEREST AND ACKNOWLEDGEMENT

We confirm that this article content has no conflicts of interest and would like to acknowledge the support of the U. S. Department of Energy under contract number DE-AC02-98CH10886.

References

[9.1] D. H. Dowell, F. K. King, R. E. Kirby *et al.*, "*In situ* cleaning of metal cathodes using a hydrogen ion beam," *Phys. Rev. ST Accel. Beams*, vol. 9, pp. 063502-1–063502-8, June, 2006.

[9.2] X. J. Wang, T. Srinivasan Rao, K. Batchelor *et al.*, "Measurements on photoelectrons from a magnesium cathode in a microwave electron gun," *Nucl. Instrum. Meth. A*, vol. 356, pp. 159-166, March 1995.

[9.3] J. Smedley, T. Rao and J. Sekutowicz, "Lead photocathodes," *Phys. Rev. ST Accel. Beams*, vol. 11, pp. 013502-1–0135022-9, January 2008.

[9.4] G. Suberlucq, "Technological challenges for high brightness photo-injectors," in *Proc. 2004 European Particle Accelerator Conf.*, 2004, pp. 64-68.

[9.5] D. H. Dowell, S. Z. Bethel and K. D. Friddell, "Results from the average power laser experiment photocathode injector test," *Nucl. Instrum. Meth. A*, vol. 356, pp. 167-176, March 1995.

[9.6] T. Rao, A. Burrill, X. Y. Chang *et al.*, "Photocathodes for energy recovery linacs," *Nucl. Instrum. Meth. A*, vol. 557, pp. 124-130, February 2006.

[9.7] C. Limborg-Deprey and P. R. Bolton, "Optimum electron distributions for space charge dominated beams in Photoinjectors," *Nucl. Instrum. Meth. A*, vol. 557, pp. 106-116, February 2006.

[9.8] O. J. Luiten, B. van der Geer, M. de Loos *et al.*, "Ideal waterbag electron bunches from an RF photogun," in *Proc. 2004 European Particle Accelerator Conf.*, 2004, pp. 725-727.

[9.9] K. Y. Lau, "Gain switching of semiconductor injection lasers," *Appl. Physics Lett.*, vol. 52, pp. 257-259, January 1988.

[9.10] M. Poelker, "High power gain-switched diode laser master oscillator and amplifier," *Appl. Physics Lett.*, vol. 67, pp. 2762-2764, November 1995.

[9.11] J. Hansknecht and M. Poelker, "Synchronous photoinjection using a frequency-doubled gain-switched fiber-coupled seed laser and ErYb-doped fiber amplifier," *Phys. Rev. ST Accel. Beams*, vol. 9, pp. 063501-1–063501-5, June 2006.

[9.12] J. M. Harris, R. W. Chrismlan and F. E. Lytle, "Pulse generation in a cw dye laser by mode-locked synchronous pumping," *Appl. Physics Lett.*, vol. 26, pp. 16-18, January 1975.

[9.13] D. L. MacFarlane and L. W. Casperson, "Pump pulse effects in synchronously pumped mode-locked dye lasers," *J. Optics Soc. America B*, vol. 6 pp. 292-299, March 1989.

[9.14] W. Koechner, *Solid-State Laser Engineering*, Berlin: Springer-Verlag, 1988, Chapter 8.

[9.15] F. J. McClung and R. W. Hellwarth, "Giant optical pulsations from ruby," *J. Appl. Physics*, vol. 33, pp. 828-829, March 1962.

[9.16] I. P. Kaminow and E. H. Turner, "Electrooptic light modulators," *Appl. Optics*, vol. 5, pp. 1612-1628, October 1966.

[9.17] C. L. Hu, "Linear electro-optic retardation schemes for the twenty classes of linear electro-optic crystals and their applications," *J. Appl. Physics*, vol. 38, pp. 3275-3284, July 1967.

[9.18] J. J. Zayhowski and C. Dill III, "Coupled-cavity electro-optically Q-switched Nd:YVO_4 microchip lasers," *Optics Lett.*, vol. 20, pp. 716-718, April 1995.

[9.19] J. Dong, A. Shirakawa, K. Takaichi *et al.*, "All-ceramic passively Q-switched Yb:YAG/Cr^{4+}:YAG microchip laser," *Electronics Lett.*, vol. 42, pp. 1154-1155, September 2006.

[9.20] G. J. Spuhler, L. Gallmann, R. Fluck *et al.*, "Passively modelocked diode-pumped erbium-ytterbium glass laser using a semiconductor saturable absorber mirror," *Electronics Lett.*, vol. 35, pp. 567-569, April 1999.

[9.21] B. H. Soffer, "Giant pulse laser operation by a passive, reversibly bleachable absorber," *J. Appl. Physics*, vol. 35, pp. 2551, 1964.

[9.22] P. Kafalas, J. I. Masters and E. M. E. Murray, "Photosensitive liquid used as a nondestructive passive Q-switch in a ruby laser," *J. Appl. Physics*, vol. 35, pp. 2349-2350, August 1964.

[9.23] PennWell 1421 S. Sheridan Road, Tulsa, OK 74112. PennWell Buyer's Guide [online]. Available: http://buyersguide.lfw.optoiq.com
[9.24] D. Mayden and R. B. Chesler, "Q-switching and cavity dumping of Nd:YAlG lasers," *J. Appl. Physics*, vol. 42, pp. 1031-1034, March 1971.
[9.25] H. Kruegle and L. Klein, "High peak power output, high PRF by cavity dumping a Nd:YAG laser," *Appl. Optics*, vol. 15, pp. 466-471.
[9.26] W. Koechner, *Solid-State Laser Engineering*, Berlin: Springer-Verlag, 1988, Chapter 9.
[9.27] A. J. De Maria, D. A. Stetser and H. Heynau, "Self mode-locking of lasers with saturable absorbers," *Appl. Physics Lett.*, vol. 8, pp. 174-176, April 1966.
[9.28] D. von der Linde, "Experimental study of single picosecond light pulses," *IEEE J. Quantum Electron.*, vol. QE-8, pp. 328-338, March 1972.
[9.29] D. Kopf, F. X. Kartner, U. Keller *et al.*, "Diode-pumped mode-locked Nd:glass lasers with an antiresonant Fabry–Perot saturable absorber," *Optics Lett.*, vol. 20, pp. 1169-1171, May 1995.
[9.30] D. J. Kuizenga and A. E. Seigman, "FM and AM mode locking of the homogeneous laser-part II: Experimental Results in a Nd:YAG laser with internal FM modulation," *IEEE J. Quantum Electron.*, vol. QE-6, pp. 709-715, November 1970.
[9.31] U. Keller, J. A. Valdmanis, M. C. Nuss *et al.*, "53 ps pulses at 1.32 μm from a harmonic mode-locked Nd:YAG laser," *IEEE J. Quantum Electron.*, vol. QE-24, pp. 427-430, February 1988.
[9.32] R. Paschotta. *Regenerative Amplifiers* [Online]. Available: http://www.rp-photonics.com/regenerative_amplifiers.html.
[9.33] D. Strickland and G. Mourou, "Compression of amplified chirped optical pulses," *Optics Commun.*, vol. 56, pp. 219-221, December 1985.
[9.34] C. Hoenninger, E. Mottay and M. Delaigue, "High Repetition Rate Ultrashort Pulse Picosecond Laser Amplifier," in *Proc. 2007 Int. Congr. Applications Lasers Electro-Optics*, 2007, Paper #M1207.
[9.35] J. L. Miller, L. A. Hackel, C. B. Dane *et al.*, "High power regenerative laser amplifier," U.S. Patent 5,285,310, February 8, 1994.
[9.36] A. Dergachev, M. A. Yakshin, P. F. Moulton *et al.*, *High-average-power picosecond drive source for photocathode injectors* [Online]. Available: http://www.qpeak.com/Meetings/CLEO-2005-PS-MOPA-d.pdf
[9.37] M. Perry. *The Amazing Power of the Petawatt* [Online]. Available: https://www.llnl.gov/str//MPerry.html
[9.38] *Vulcan Home Page* [Online]. Available: http://www.clf.rl.ac.uk/Facilities/Vulcan/12248.aspx
[9.39] X. Wei, Q. Zhu, X. Huang *et al.*, "Recent progress and future prospects of high-energy petawatt laser in LFRC, CAEP," in *Journal Physics: Conf. Series*, vol. 112, 2008, pp. 032011.
[9.40] E. Wolf, Ed., *Progress in Optics*, Vol. 34, Amsterdam: Elsevier Science, 2004.
[9.41] Lumera Laser GmbH, Opelstr. 10, 67661 Kaiserslautern, Germany.
[9.42] S. Schreiber, I. Will, D. Sertore *et al.*, "Running experience with the laser system for the RF gun based injector at the TESLA Test Facility linac," *Nucl. Instrum. Meth. A*, vol. 445, pp. 427-431, May 2000.
[9.43] I. Will, G. Kross and I. Templin, "The upgraded photocathode laser of the TESLA Test Facility," *Nucl. Instrum. Meth. A*, vol. 541, pp. 467-477, April 2005.
[9.44] V. Yakimenko. (2007, December 7). *Multi-Pulse Nd:YAG Laser Schematic Layout* [Online]. Available: http://www.bnl.gov/atf/core_capabilities/yaglayout.asp.
[9.45] M. Shinn. (2005, March 22). *Drive laser state-of-the-art: Performance, stability and programmable repetition rate* [Online]. Available: http://www.jlab.org/intralab/calendar/archive04/erl/talks/WG1/WG1_Shinn_Tue_0830.pdf

[9.46] A. Sakumi, "Synchronization between laser and electron beam at photocathode RF gun," in *Proc. 2005 Particle Accelerator Conf.*, 2005, pp. 3079-3081.

[9.47] P. F. Moulton, "Pulse-pumped operation of divalent transition-metal lasers," *IEEE J. Quantum Electron.*, vol. QE-18, pp. 1185-1188, August 1982.

[9.48] T. Brabec, Ch. Speilmann, P. F. Curley *et al.*, "Kerr lens mode locking," *Optics Lett.*, vol. 17, pp. 1292-1294, September 1992.

[9.49] L. Y. Liu, J. M. Huxley, E. P. Ippen *et al.*, "Self-starting additive-pulse mode locking of a Nd:YAG laser," *Optics Lett.*, vol. 15, pp. 553-555, May 1990.

[9.50] J. F. Wishart, A. R. Cook and J. R. Miller, "The LEAF picosecond pulse radialysis facility at Brookhaven National Laboratory," *Rev. Sci. Instrum.*, vol. 75, pp. 4359-4366, November 2004.

[9.51] I. Wilke, A. M. MacLeod, W. A. Gillespie *et al.*, "Single-shot electron-beam bunch length measurements," *Phys. Rev. Lett.*, vol. 88, pp. 124801-1–124801-4, March 2002.

[9.52] E. Fill, L. Veisz, A. Apolonski *et al.*, "Sub-fs electron pulses for ultrafast electron diffraction," *New J. Physics*, vol. 8, pp. 272-1–272-11, November 2006.

[9.53] T. Tsang, "Multiple-harmonic generation on ZnO nanocrystalline film," in *Tech. Dig, Lasers Electro-Optics/Quantum Electronics Laser Science and Photonic Applications Systems Technologies Conf.*, 2005, pp. 2103-2104.

[9.54] O. E. Martinez, "3000 times grating compressor with positive group velocity dispersion: Application to fiber compensation in 1.3-1.6 μm region," *IEEE J. Quantum Electron.*, vol. 23, pp. 59-64, January 1987.

[9.55] E. B. Treacy, "Optical pulse compression with diffraction gratings," *IEEE J. Quantum Electron.*, vol. 5, pp. 454-458, September 1969.

[9.56] A. Offner, "Unit power imaging catoptric anastigmat," U.S. Patent 3,748,015, June 21, 1971.

[9.57] G. Cheriaux, P. Rousseau, F. Salin *et al.*, "Aberration-free stretcher design for ultrashort-pulse amplification," *Optics Lett.*, vol. 21, pp. 414-416, March 1996.

[9.58] E. Miesak and R. Negres, "Alignment procedure for a dual grating pulse compressor," *Appl. Optics*, vol. 37, pp. 8146-8147, 1998.

[9.59] A. V. Tarasishin, S. A. Magnitskii and A. M. Zheltikov, "Matching phase and group velocities in second-harmonic generation in finite one-dimesnsional photonic band-gap structures," *Laser Physics*, vol. 11, pp. 31-38, 2001.

[9.60] B. A. Richman, S. E. Bisson, R. Trebino *et al.*, "Recent advances in achromatic phase matching for tunable and ultrashort second-harmonic generations," in *Tech. Dig. 1998 Conf. Lasers Electro-Optics*, 1998, pp. 105.

[9.61] P. Wasylczyk, I. A. Walmsley, W. Wasilewski *et al.*, "Broadband noncollinear optical parametric amplifier using a single crystal," *Optics Lett.*, vol. 30, pp. 1704-1706, July 2005.

[9.62] R. Akre, J. Castro, Y. Ding *et al.*, "Initial commissioning experience with the LCLS injector," in *Proc. 2007 Particle Accelerator Conf.*, 2007, pp. 1302-1304.

[9.63] J. M. Byrd, L. Doolittle, G. Huang *et al.*, "Femtosecond synchronization of laser system for the LCLS," in *Proc. 2010 Int. Particle Accelerator Conf.*, 2010, pp. 58-60.

[9.64] SPARC General Info [Online]. Available: http://www.lnf.infn.it/acceleratori/sparc/

[9.65] P. Musumeci. (2009, November). *Ultrashort laser pulses on the cathode: blow-out regime and multiphoton photoemission* [Online]. Available: http://pbpl.physics.ucla.edu/HBEB/PlenaryTalks/MUSUMECI.pdf

[9.66] P. Musumeci, L. Cultrera, M. Ferrario *et al.*, "Multiphoton photoemission from a copper cathode illuminated by ultrashort laser pulses in an rf photoinjector," *Phys. Rev. Lett.*, vol. 104, pp. 084801-1–084801-4, February 2010.

[9.67] D. A. Grukh, V. A. Bogatyrev, A. A. Sysolyatin *et al.*, "Broadband radiation source based on ytterbium-doped fibre with fibre-length-distributed pumping," *Quantum Electron.*, vol. 34, pp. 247-248, 2004.

[9.68] A. Bellemare, M. Karásek, C. Riviere *et al.*, "A broadly tunable Erbium-doped fiber ring laser: Experimentation and modeling," *IEEE J. Selected Topics Quantum Electron.*, vol. 7, pp. 22-29, January 2001.

[9.69] A. Tünnermann, T. Schreiber and J. Limpert, "Fiber lasers and amplifiers: An ultrafast performance evolution," *Appl. Optics*, vol. 49, pp. F71-F78, September 2010.

[9.70] M. Nakazawa, Y. Kimura and K. Suzuki, "An ultra-efficient, erbium-doped fiber amplifier of 10.2 dB/mW at 0.98 μm pumping and 5.1 dB/mW at 1.48 μm pumping," in *Proc. Topical Meeting Optical Amplifiers Applications*, 1990, pp. PDP1-1–PDP1-4.

[9.71] A. Liu and K. Ueda, "The absorption characteristics of circular, offset, and rectangular double-clad fibers," *Optics Commun.*, vol. 132, pp. 511-518, December 1996.

[9.72] J. P. Koplow, D. D. A. V. Kliner *et al.*, "Single-mode operation of a coiled multimode amplifier," *Optics Lett.*, vol. 25, pp. 442-444, April 2000.

[9.73] J. Limpert, A. Liem, M. Reich *et al.*, "Low-nonlinearity single-transverse-mode ytterbium-doped photonic crystal fiber amplifier," *Optics Express*, vol. 12, pp. 1313-1319, April 2004.

[9.74] D. G. Ouzounov, I. V. Bazarov, B. M. Dunham *et al.*, "The laser system for the ERL electron source at Cornell University," in *Proc. 2007 Particle Accelerator Conf.*, 2007, pp. 530-532.

[9.75] P. Madasamy, L. Coressel, D. R. Jander *et al.*, "Tunable pulse width, short pulse high power green laser," presented at Conf. Lasers Electro-Optics, 2010.

[9.76] M. Nakazawa and E. Yoshida, "A 40-GHz 850-fs regeneratively FM mode-locked polarization-maintaining erbium doped fiber ring laser," *IEEE Photonics Tech. Lett.*, vol. 12, pp. 1613-1615, December 2000.

[9.77] A. B. Rulkov, M. Y. Vyatkin, S. V. Popov *et al.*, "High brightness picosecond all-fiber generation in 525-1800 nm range with picosecond Yb pumping," *Optics Express*, vol. 13, pp. 377-381, January 2005.

[9.78] M. H. Ober, M. Hofer, U. Keller *et al.*, "Self-starting diode-pumped femtosecond Nd fiber laser," *Optics Lett.*, vol. 18, pp. 1532-1534, September 1993.

[9.79] H. Schlüter, C. Tillkorn, U. Bonna *et al.*, "Dense spatial multiplexing enables high brightness multi-kW diode laser systems," in *Proc. SPIE – High-power Diode Laser Technology Applications IV*, 2006, vol. 6104, pp. 61040M-1–61040M-8.

[9.80] M. Ziad, M. Al-Haiari and W. Khalid. (2006). *Optical Caples* [Online]. Available: FTP: http://dar.ju.edu.jo Directory: mansour/optical/729projects/ File: fiber connections.doc

[9.81] C. Limborg-Deprey and H. Tomizawa, "Maximizing brightness in photoinjector," in *Proc. 46th Physics Applications of High Brightness Electron Beams Workshop*, 2007, pp. 174-193.

[9.82] J. Luiten, B. van der Geer, M. de Loos *et al.*, "Ideal waterbag electron bunches from an RF photogun," in *Proc 2004 European Particle Accelerator Conf.*, 2004, pp. 725-727.

[9.83] Y. Li and X. Chang, "Generation of ellipsoidal beam through 3D pulse shaping for a photoinjector drive laser," in *Proc. 2006 Int. Linear Accelerator Conf.*, 2006, pp. 776-778.

[9.84] O. J. Luiten, S. B. van der Geer, M. J. de Loos *et al.*, "How to realize uniform three-dimensional ellipsoidal electron bunches," *Phys. Rev. Lett.*, vol. 93, pp. 094802-1–094802-4, August 2004.

[9.85] P. Musumeci, J. T. Moody, R. J. England *et al.*, "Experimental generation and characterization of uniformly filled ellipsoidal electron-beam distributions," *Phys. Rev. Lett.*, vol. 100, pp. 244801-1–244801-4, June 2008.

[9.86] H. Tomizawa, H. Dewa, T. Taniuchi *et al.*, "Adaptive shaping system for both spatial and temporal profiles of a highly stabilized UV laser light source for a photocathode RF gun," *Nucl. Instrum. Meth A*, vol. 557, pp. 117-123, February 2006.

[9.87] I. Will and G. Klemz, "Generation of flat-top picosecond pulses by coherent pulse stacking in a multicrystal birefringent filter," *Optics Express*, vol. 16, pp. 14922-14937, September 2008.

[9.88] C. Limborg-Deprey and H. Tomizawa, "Maximizing brightness in photoinjectors," *Int. J. Modern Physics A*, vol. 22, pp. 3864-3881, 2007.

[9.89] D. Garzella, O. Gobert, Ph. Hollander *et al.*, "Temporal analysis and shape control of UV high energy laser pulses for photoinjectors," in *Proc. 2006 Free Electron Laser*, 2006, p. 552-555.

[9.90] A. Yariv and P. Yeh, *Optical Waves in Crystals: Propagation and Control of Laser Radiation*, New York: John Wiley & Sons, 1984.

[9.91] A. M. Weiner, "Femtosecond pulse shaping using spatial light modulators," *Rev. Sci. Instrum.*, vol. 71, pp. 1929-1960, May 2000.

[9.92] A. M. Weiner, J. P. Heritage and E. M. Kirschner, "High-resolution femtosecond pulse shaping," *J. Optics Soc. America B*, vol. 5, pp. 1563-1572, August 1988.

[9.93] S. Cialdi, C. Vicario, M. Petrarca *et al.*, "Simple scheme for ultraviolet time-pulse shaping," *Appl. Optics*, vol. 46, pp. 4959-4962, August 2007.

[9.94] J. Yang, F. Sakai, T. Yanagida *et al.*, "Low-emittance electron-beam generation with laser pulse shaping in photocathode radio-frequency gun," *J. Appl. Physics*, vol. 92, pp. 1608-1612, August 2002.

[9.95] R. Akre, D. Dowell, P. Emma *et al.*, "Commissioning the Linac Coherent Light Source injector," *Phys. Rev. ST Accel. Beams*, vol. 11, pp. 30703-1–30703-20, March 2008.

[9.96] C. Vicario, A. Ghigo, M. Petrarca *et al.*, "Laser temporal pulse shaping experiment for SPARC photoinjector," in *Proc. 2004 European Particle Accelerator Conf.*, 2004, pp. 1300-1302.

[9.97] H. Loos, M. Boscolo, D. Dowell *et al.*, "Temporal E-beam shaping in an S-band accelerator," in *Proc. 2005 Particle Accelerator Conf.*, 2005, pp. 642-644.

[9.98] C. W. Siders, J. L. W. Siders, A. J. Taylor *et al.*, "Efficient high-energy pulse-train generation using a 2^n-pulse Michelson interferometer," *Appl. Optics*, vol. 37, pp. 5302-5305, August 1998.

[9.99] S. Zhou, D. Ouzounov, H. Li *et al.*, "Efficient temporal shaping of ultrashort pulses with birefringent crystals," *Appl. Optics*, vol. 46, pp. 8488-8492, December 2007.

[9.100] I. V. Bazarov, D. G. Ouzounov, B. M. Dunham *et al.*, "Efficient temporal shaping of electron distributions for high-brightness photoemission electron guns," *Phys. Rev. ST Accel. Beams*, vol. 11, pp. 40702-1–040702-6, April 2008.

[9.101] A. K. Sharma, T. Tsang and T. Rao, "Theoretical and experimental study of passive spatiotemporal shaping of picosecond laser pulses," *Phys. Rev. ST Accel. Beams*, vol. 12, pp. 33501-1–33501-9, March 2009.

[9.102] I. Will, "Generation of flat-top picosecond pulses by means of a two-stage birefringent filter," *Nucl. Instrum. Meth. A*, vol., pp. 119-125, July 2008.

[9.103] Y. Park, M. H. Asghari, T. J. Ahn *et al.*, "Transform-limited picosecond pulse shaping based on temporal coherence synthesization," *Optical Express*, vol. 15, pp. 9584-9599, July 2007.

[9.104] S. P. Chang, J. Kuo, Y. Lee *et al.*, "Transformation of Gaussian to coherent uniform beams by inverse-Gaussian transmittive filters," *Appl. Optics*, vol. 37, pp. 747-752, February 1998.

[9.105] M. Yun, M. Wang, Q. Wang *et al.*, "Laser beam shaping system with a radial birefringent filter," *J. Modern Optics*, vol. 54, pp. 129-136, January 2007.

[9.106] X. Tan, B. Gu, G. Yang *et al.*, "Diffractive phase elements for beam shaping: A new design method," *Appl. Optics*, vol. 34, pp. 1314-1320, March 1995.

[9.107] P. W. Rhodes and D. L. Shealy, "Refractive optical systems for irradiance redistribution of collimated radiation: Their design and analysis," *Appl. Optics*, vol. 19, pp. 3545-3553, October 1980.

[9.108] J. A. Hoffnagle and C. M. Jefferson, "Design and performance of a refractive optical system that converts a Gaussian to a flattop beam," *Appl. Optics*, vol. 39, pp. 5488-5499, October 2000.

[9.109] T. Takaoka, N. Kawano, Y. Awatsuji *et al.*, "Design of a reflective aspherical surface of a compact beam-shaping device," *Optical Rev.*, vol. 13, pp. 77-86, March 2006.

[9.110] Y. Li and J. W. Lewellen, "Generating a quasiellipsoidal electron beam by 3D laser-pulse shaping," *Phys. Rev. Lett.*, vol. 100, pp. 074801-1–074801-4, February 2008.

[9.111] S. Zhang, S. Benson, J. Gubeli *et al.*, "Investigation and evaluation on pulse stackers for temporal shaping of laser pulses," in *Proc. 32nd Int. Free Electron Linac Conf.*, 2010, pp. 394-397.

[9.112] Y. Li, S. Chemerisov and J. Lewellen, "Laser pulse shaping for generating uniform three-dimensional ellipsoidal electron beams," *Phys. Rev. ST Accel. Beams*, vol. 12, pp. 020702-1–020702-11, February 2009.

[9.113] M. Bellaveglia, A. Gallo and C. Vicario, "SPARC photo-injector synchronization system and time jitter measurement," LNF of INFN, Roma, Italy, EUROFEL-Report-2006-DS3-027, 2006.

[9.114] D. von der Linde, "Characterization of the noise in continuously operating mode-locked lasers," *Appl. Physics B*, vol. 39, pp. 201-217, April 1986.

[9.115] J. Kim, J. Chen, Z. Zhang *et al.*, "Long-term femtosecond timing link stabilization using a single-crystal balanced cross correlator," *Optics Lett.*, vol. 32, pp. 1044-1046, May 2007.